Cell Reports

Article

Aryl hydrocarbon receptor signals in epithelial cells govern the recruitment and location of Helios^{+} Tregs in the gut

Graphical abstract

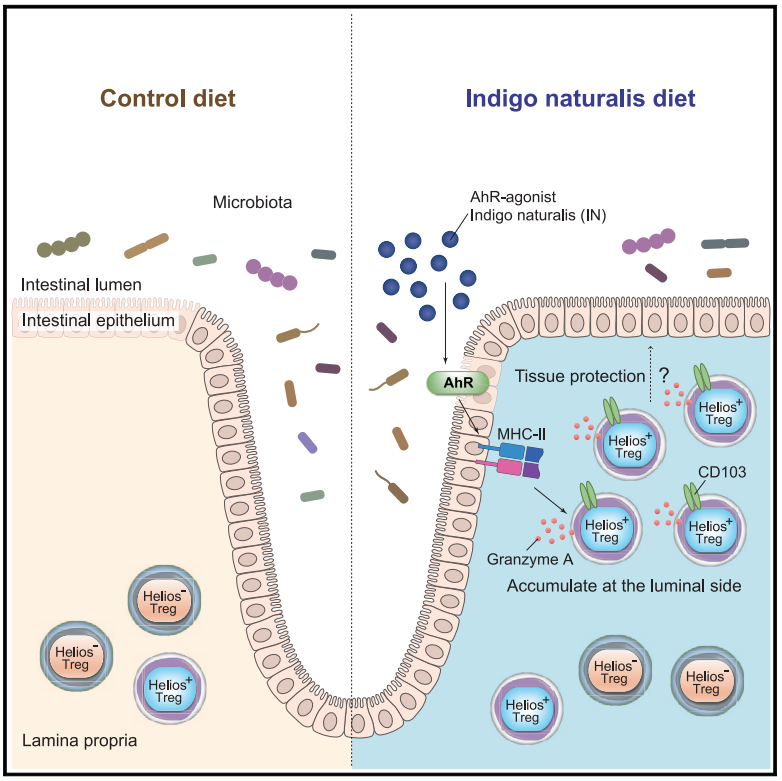

Highlights

- Indigo naturalis (IN) increases Helios^{+} Tregs in the colon
- IN-induced Tregs are localized near the crypt top in the colon
- AhR signaling in colonic epithelial cells is indispensable for Treg accumulation
- IN treatment induces colonic Tregs and suppresses experimental colitis

Authors

Yusuke Yoshimatsu, Tomohisa Sujino, Kentaro Miyamoto, ..., Takeshi Imamura, Akihiko Yoshimura, Takanori Kanai

Correspondence

tsujino1224@keio.jp (T.S.), takagast@keio.jp (T.K.)

In brief

Yoshimatsu et al. show that aryl hydrocarbon receptor (AhR) signaling in ECs governs the induction and localization of indigo naturalis (IN)-induced Helios^{+} Tregs in the colon both in the murine model and in ulcerative colitis patients.

Yoshimatsu et al., 2022, Cell Reports *39*, 110773
May 10, 2022
https://doi.org/10.1016/j.celrep.2022.110773

CellPress

Cell Reports

CellPress
OPEN ACCESS

Article

Aryl hydrocarbon receptor signals in epithelial cells govern the recruitment and location of Helios$^+$ Tregs in the gut

Yusuke Yoshimatsu,[1,7] Tomohisa Sujino,[2,8,*] Kentaro Miyamoto,[1,3,7] Yosuke Harada,[1,7] Shun Tanemoto,[1] Keiko Ono,[1] Satoko Umeda,[1] Kosuke Yoshida,[1] Toshiaki Teratani,[1] Takahiro Suzuki,[1,3] Yohei Mikami,[1] Nobuhiro Nakamoto,[1] Nobuo Sasaki,[4] Kaoru Takabayashi,[2] Naoki Hosoe,[2] Haruhiko Ogata,[2] Kazuaki Sawada,[5] Takeshi Imamura,[5] Akihiko Yoshimura,[6] and Takanori Kanai[1,*]

[1]Division of Gastroenterology and Hepatology, Department of Internal Medicine, Keio University School of Medicine, Tokyo, Japan
[2]Center for Diagnostic and Therapeutic Endoscopy, Keio University School of Medicine, Tokyo, Japan
[3]Miyarisan Pharmaceutical Co., Ltd., Tokyo, Japan
[4]Institute of Molecular and Cellular Regulation, Gunma University, Maebashi, Japan
[5]Department of Molecular Medicine for Pathogenesis, Ehime University, Toon, Japan
[6]Department of Microbiology and Immunology, Keio University School of Medicine, Tokyo, Japan
[7]These authors contributed equally
[8]Lead contact
*Correspondence: tsujino1224@keio.jp (T.S.), takagast@keio.jp (T.K.)
https://doi.org/10.1016/j.celrep.2022.110773

SUMMARY

CD4$^+$Foxp3$^+$ regulatory T cells (Tregs) are essential for homeostasis in the colon, but the mechanism by which local environmental cues determine the localization of colonic Tregs is unclear. Here, we administer indigo naturalis (IN), a nontoxic phytochemical aryl hydrocarbon receptor (AhR) agonist used for treating patients with ulcerative colitis (UC) in Asia, and we show that IN increases Helios$^+$ Tregs and MHC class II$^+$ epithelial cells (ECs) in the colon. Interactions between Tregs and MHC class II$^+$ ECs occur mainly near the crypt bottom in the steady state, whereas Tregs dramatically increase and shift toward the crypt top following IN treatment. Moreover, the number of CD25$^+$ T cells is increased near the surface of ECs in IN-treated UC patients compared with that in patients treated with other therapies. We also highlight additional AhR-signaling mechanisms in intestinal ECs that determine the accumulation and localization of Helios$^+$ Tregs in the colon.

INTRODUCTION

Intestinal homeostasis is the balance between pathogenic T cells and anti-inflammatory T cells induced by food- or microbiome-derived antigens or the microbiome itself (Belkaid and Hand, 2014; Honda and Littman, 2016; Kamada et al., 2013). To achieve and maintain intestinal homeostasis, CD4$^+$Foxp3$^+$ regulatory T cells (Tregs) suppress intestinal inflammation in mammalian species (Atarashi et al., 2011; Brunkow et al., 2001; Hori et al., 2003; Sakaguchi et al., 2013) by inhibiting several other types of immune cells through anti-inflammatory cytokines, such as interleukin (IL)-10, and cell surface proteins, such as CD25 and cytotoxic T lymphocyte-associated antigen 4 (CTLA-4). Tregs are essential to maintain homeostasis in the intestine and are induced by various factors (Brunkow et al., 2001; Hori et al., 2003). Based on the expression patterns of key transcription factors in addition to Foxp3, Tregs are classified into thymus-derived natural Tregs (thymic Tregs, tTregs) and peripheral Tregs (pTregs). Helios$^+$ tTregs are primarily generated in the thymus and distributed throughout the entire body from birth to protect against autoimmune diseases (Littman and Rudensky, 2010; Ohkura et al., 2013; Sakaguchi et al., 2008). In peripheral tissues, GATA3-expressing tTregs respond to IL-33 through the IL-33 receptor ST2 and contribute to immune suppression and tissue repair (Schiering et al., 2014; Wohlfert et al., 2011), whereas pTregs are most abundant in the intestine and induced by intestinal bacteria or bacteria-derived metabolites (Atarashi et al., 2011; Kashiwagi et al., 2015; Nutsch et al., 2016; Sakaguchi et al., 2008; Sefik et al., 2015; Yoshimura and Muto, 2011) and food antigens (Kim et al., 2016). In particular, the tryptophan catabolite kynurenine activates aryl hydrocarbon receptors (AhRs) in dendritic cells and enhances the generation of pTregs (Mezrich et al., 2010), and Treg-specific deletion of *Ahr* reduces pTregs but not tTregs *in vivo* (Ye et al., 2017). A decrease in microbiota-derived AhR agonists was observed in inflammatory bowel disease (IBD) patients with a mutation in the *CARD9* gene, an IBD susceptibility gene (Lamas et al., 2016), supporting the hypothesis that AhR ligands maintain immunological homeostasis in the gut. The nontoxic AhR ligand 2-(1′H-indole-3′-carbonyl)-thiazole-4-carboxylic acid methyl ester ameliorates 2,4,6-trinitrobenzenesulfonic acid-induced colitis mediated by human CD4$^+$ T cells by increasing the number of Tregs (Goettel et al., 2016). In addition, indigo naturalis (IN) is a phytochemical compound containing indole derivatives, such as indigo, indirubin, and indole-3-aldehyde. IN is generated through

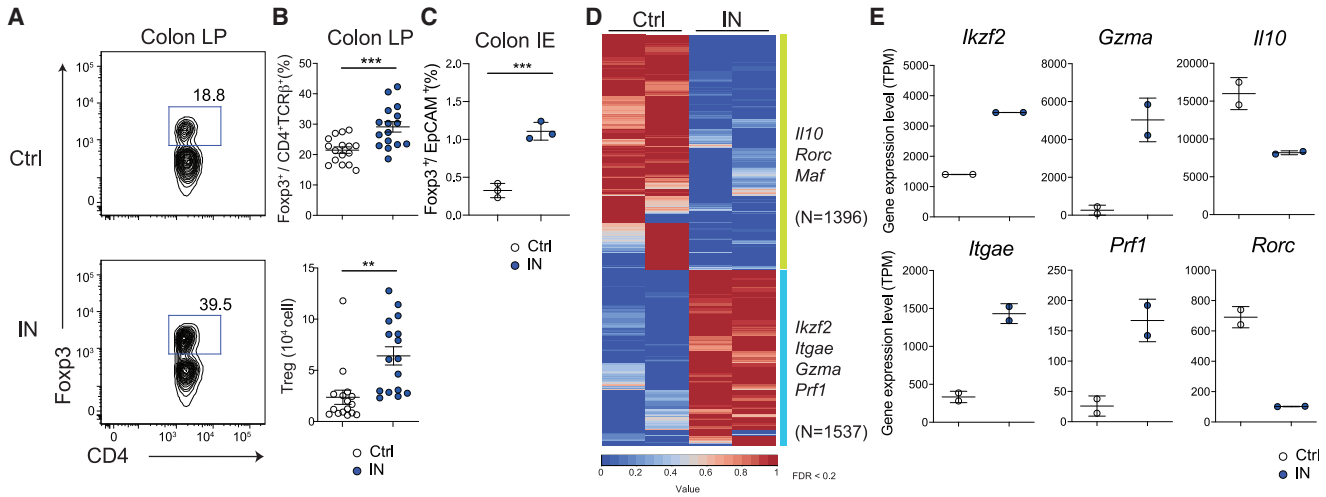

Figure 1. IN specifically induced Tregs in colon, which have CTL-like characteristics

(A) C57BL/6J mice of 7 weeks received CE2 diet (Ctrl diet) or CE2 with 4% indigo naturalis (IN) (IN diet) for 3 weeks (n = 16/group). Representative flow cytometry plots of Foxp3 expression by CD4 positive lymphocytes in colon lamina propria (cLP).

(B) Percentage of Foxp3$^+$ cells (Treg cells) among CD4$^+$TCRβ$^+$ lymphocyte subsets and number of Treg cells in cLP.

(C) Ratio of Tregs to EpCAM$^+$ cells obtained from colon intestinal epithelial cells (cIE) (n = 3/group).

(D and E) *Rosa26*$^{lsl\text{-}tdTomato}$; *Foxp3*$^{eGFP\text{-}Cre\text{-}ERT2}$ mice received Ctrl diet or IN diet for 3 weeks (n = 2/group), followed by being treated with TAM administration, and Tomato$^+$ CD4$^+$ T cells from cLP were sorted for bulk RNA-seq. Heatmap of the top differentially expressed genes classified by sorted cells in Ctrl group and IN group (D) and representative gene expression level of target cells in each group presented as bar graph (E). p values obtained via by Student's t test. **<0.01, ***<0.001. Data are shown as mean ± SEM (B) or ± SD (C) of individual mice (n = 16 for B, n = 3 for C), representative of two independent experiments.

a fermentation process (Hsu et al., 2018; Sugimoto et al., 2016a) and has recently been applied clinically as an AhR agonist for treating refractory ulcerative colitis (UC) (Naganuma et al., 2018; Sugimoto et al., 2016b; Yoshimatsu et al., 2020). The efficacy of IN is 65%–75%, which is equivalent to that of anti-TNFα agents and corticosteroids (Rutgeerts et al., 2005; Turner et al., 2007). Although the effects of AhR ligands on pTregs or other immune cells have been investigated (Gutiérrez-Vázquez and Quintana, 2018; Qiu et al., 2012; Quintana et al., 2008, 2010; Stockinger et al., 2014; Ye et al., 2017), the mechanisms by which the complex network of endogenous and exogenous AhR ligands in the intestine regulates intestinal Tregs remain unclear.

In this study, we found that exposure to an IN diet containing AhR agonists increased GATA3^{lo} Helios$^+$ RORγt$^-$ Tregs in the colon (IN-Tregs), depending on the gut microbiota. Single-cell (sc) transcriptomic analysis of Tregs revealed an increased repertoire of T cell receptors (TCRs) in IN-Tregs. These Tregs were located next to MHC class II-positive epithelial cells (ECs) near the luminal side in IN-fed mice, and CD25$^+$ T cells were located near the luminal side of the colon in UC patients treated with IN. AhR signaling in ECs but not T cells governed the increased number of Tregs and their localization in the colon. Our findings provide evidence that AhR signaling in ECs increases Tregs, with alterations in their transcriptomic profiles and localization.

RESULTS

IN increases Helios$^+$ Tregs in the colon

IN, a phytochemical AhR agonist, is used for the treatment of chronic intestinal inflammation; however, its anti-inflammatory role in the gut has not been elucidated. To address this question, we profiled the intestinal immune cells of mice fed IN (IN-fed mice) for 3 weeks. Consistent with previous reports (Xiao et al., 2015), we confirmed the IN-induced activation of AhR signaling via the upregulation of *Cyp1a1* expression, a downstream target of AhR signaling, by qPCR (Figure S1A). The composition of intestinal immune cells, including IL-22-producing type 3 innate lymphoid cells, T helper 1 (Th1), Th17, B cells, MHC class II$^+$ antigen-presenting cells, macrophages, and neutrophils (Figures S1B–S1F), was not dramatically altered. However, the total number of Foxp3$^+$ Tregs was significantly increased in the intraepithelial compartment and lamina propria of the colon (Figures 1A–1C) and spleen (Figure S1G), but not the small intestine or mesenteric lymph nodes (Figures S1H and S1I), in IN-fed mice compared with the number in mice fed a CE2 diet (control diet) (Ctrl-fed mice).

To characterize the phenotype of increased Tregs in IN-fed mice, we next compared the transcriptome of colonic CD4$^+$TCRβ$^+$Tomato$^+$ Tregs from tamoxifen-inducible *Foxp3*$^{eGFP\text{-}Cre\text{-}ERT2}$:*Rosa26*$^{lsl\text{-}tdtomato}$ (iFoxp3^{Tomato}) mice fed IN or a Ctrl diet by RNA sequencing (RNA-seq) (referred to as IN-Tregs and Ctrl-Tregs). With a false discovery rate cutoff of <0.2, 1,537 and 1,396 genes were highly expressed in IN-Tregs and Ctrl-Tregs, respectively (Figure 1D). In particular, IN-Tregs were characterized by higher expression levels of *Ikzf2* (encoding Helios), *Gzma* (encoding granzyme A), *Itgae* (encoding CD103), and *Prf1* (encoding perforin-1), whereas Ctrl-Tregs were associated with pTregs with increased expression of *Il10*, *Rorc*, and *Maf* (Whibley et al., 2019) (Figures 1D and 1E).

These findings were further validated by flow cytometry analysis. The results showed that IN-Tregs were mainly

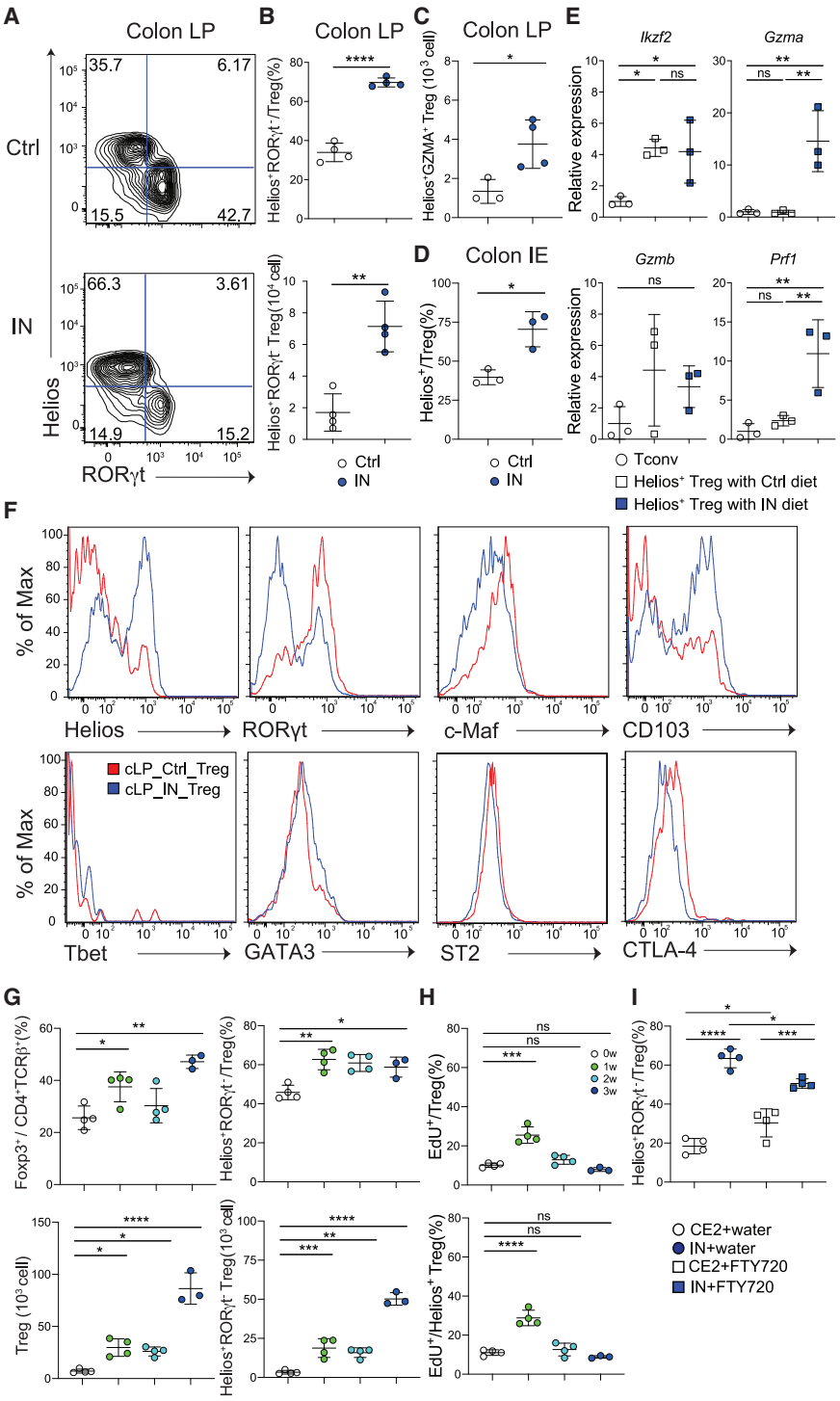

Figure 2. IN accumulates Helios$^+$ RORγt$^-$ Tregs in colon, allowing Helios$^+$ RORγt$^-$ Tregs to proliferate in the colon within a week and then remain in the colon

(A–D) C57BL/6J mice of 7 weeks received CE2 diet (Ctrl diet) or CE2 with 4% indigo naturalis (IN) (IN diet) for 3 weeks. Representative flow cytometry plots of Helios and RORγt$^-$ expression by Treg cells in colon lamina propria (cLP) (A). Percentage of Helios$^+$ RORγt$^-$ cells among Treg cells and number of Helios$^+$ RORγt$^-$ Treg cells in cLP (B) and that of Helios$^+$ Treg cells among Treg cells in colon intestinal epithelia (cIE) (C). Number of Helios$^+$ GZMA$^+$ cells among Tregs are shown (D). (E) *Helios*^{Venus}:*Rosa26*$^{lsl\text{-}tdTomato}$;*Foxp3*$^{eGFP\text{-}Cre\text{-}ERT2}$ mice received Ctrl diet or IN diet for 3 weeks, followed by being treated with TAM administration. Venus$^+$ Tomato$^+$ CD4$^+$ T cells and Tomato$^-$ CD4$^+$ Tcells (Tconv) from cLP were sorted for qPCR. The mRNA expression of indicated genes in them were measured. qRT-PCR was performed in triplicate for individual mice, and *Ct* values obtained were normalized to *Rpl32*.

(F) C57BL/6J mice of 7 weeks received Ctrl diet or IN diet for 3 weeks. Phenotype analysis of Ctrl-Tregs and IN-Tregs. Representative histograms gated on colonic Tregs are shown.

(G and H) C57BL/6J mice of 7 weeks received Ctrl diet or IN diet for 1, 2, or 3 weeks. EdU (400 μg/day) was administered intraperitoneally to them consecutively 3 days from 2 days to 1 h before the date of sacrifice. Percentage of Foxp3$^+$ cells (Tregs) among CD4$^+$TCRβ$^+$ lymphocyte subsets, Helios$^+$ RORγt$^-$ cells among Treg cells, and number of them are shown (G). Percentage of EdU$^+$ cells among Tregs and Helios$^+$ RORγt$^-$ Treg cells are shown (H).

(I) C57BL/6J mice of 7 weeks received Ctrl diet or IN diet for 3 weeks. FTY720 (1 mg/kg) or water was also administered orally to them once a day from the start date of the special feedings. Percentage of Helios$^+$ RORγt$^-$ cells among Treg cells are shown. p values obtained via by Student's t test (B-D) and one-way ANOVA with Tukey's post hoc test (E and G–I). *<0.05, **<0.01, ***<0.001, ****<0.0001. ns: not significant. Data are shown as mean ± SD of individual mice (n = 3–4), representative of two independent experiments.

composed of Helios$^+$ Tregs and Helios$^+$GZMA$^+$ Tregs, with an approximately 4-fold increase compared with Ctrl-Tregs in the lamina propria (Figures 2A–2C) and intraepithelial compartment in the colon (Figure 2D) but not the spleen, small intestine, or mesenteric lymph nodes (Figures S2A–S2C). We next examined the expression of *Gzma* and *Prf1* in IN-Helios$^+$ Tregs and Ctrl-Helios$^+$ Tregs. To this end, we crossed *Helios*^{Venus} mice with iFoxp3^{Tomato} mice to generate a dual reporter of Helios and Foxp3 expression (*Helios*^{Venus}:i*Foxp3*^{Tomato} mice) and evaluated mRNA expression in colonic Helios$^+$Foxp3$^+$ Tregs sorted as Venus$^+$Tomato$^+$ cells from *Helios*^{Venus}:i*Foxp3*^{Tomato} mice fed IN or a Ctrl diet. As expected, Helios$^+$Foxp3$^+$ Tregs expressed higher levels of the cytotoxic genes *Gzma* and *Prf1* in IN-fed mice compared with those in Ctrl-fed mice (Figure 2E).

Given that IN-Tregs display a Helios$^+$ tTreg phenotype with cytolytic activity (*Gzma* and *Prf1*) (Raffin et al., 2020; Shevach,

2009), we next examined markers of tTregs and pTregs. Flow cytometric analysis revealed that IN-Tregs expressed high levels of Helios and the tissue-resident cell marker CD103 (Annacker et al., 2005) but low levels of the pTreg markers RORγt and c-MAF (Xu et al., 2018) and other lineage-determining transcription factors, including GATA3 and T-bet (Yu et al., 2015) (Figures 2F and S2D–S2F). GATA3^{+} tTregs express ST2, respond to tissue damage following IL-33 stimulation, and contribute to tissue repair (Schiering et al., 2014; Wohlfert et al., 2011). However, the expression levels of ST2 in Tregs (Figures 2F, S2G, and S2H) and its ligand *Il33* in whole colon tissues or colon ECs were not induced in IN-fed mice (Figure S2I). Taken together, IN-Tregs express high levels of Helios and low levels of RORγt, similar to tTregs, but they do not express other tTreg makers, such as ST2 and GATA3.

We next questioned whether IN-Tregs proliferate in the colon or migrate from other organs. First, we analyzed the kinetics of Tregs in IN-fed mice and found that total Tregs and Helios^{+}RORγt^{-} Tregs accumulated in the colon 2–3 weeks after IN diet exposure (Figure 2G). We then evaluated the incorporation of 5-ethynyl-2′-deoxyuridine (EdU) in Tregs at each time point. The percentage of EdU^{+} cells in Tregs and Helios^{+} Tregs was significantly increased at 1 week after IN diet exposure, but the percentage of EdU^{+} cells at weeks 2 and 3 was similar to that at baseline (Figure 2H). In contrast, the percentage of EdU^{+} cells in RORγt^{+} Tregs was comparable throughout the 3 weeks of IN feeding (Figure S2J). We next explored the possibility that Tregs migrate to the colon from mesenteric lymph nodes in IN-fed mice. We evaluated the number of Tregs in IN-fed mice treated in the presence or absence of FTY720. FTY720 slightly increased the percentage of Helios^{+}RORγt^{-} cells in Tregs in wild-type (WT) mice. Although the percentage of Helios^{+}RORγt^{-} cells in colonic Tregs of IN-fed mice treated with FTY720 was decreased compared with that in IN-fed mice without FTY720, the percentage of Helios^{+}RORγt^{-} cells in Tregs in FTY720-treated IN-fed mice was significantly increased compared with that in FTY720-treated Ctrl-diet mice (Figure 2I). These data suggest that some IN-Tregs do not originate from secondary lymphoid organs. Furthermore, to consider the possibility that IN induces the differentiation of Helios^{+}RORγt^{-} Tregs from naive T cells, we transferred naive T cells to *Rag2*$^{-/-}$ mice fed the IN or Ctrl diet. The proportions of total and Helios^{+}RORγt^{-} Tregs were not significantly different between *Rag2*$^{-/-}$ mice fed Ctrl and IN diets (Figure S2K), suggesting that IN did not promote naive T cell differentiation into Helios^{+}RORγt^{-} Tregs in the gut. Taken together, these data suggest that IN may orchestrate the expansion and recruitment of colonic Tregs with a tissue-resident tTreg phenotype.

Characteristics of Tregs induced by the AhR agonist IN

To gain a deeper insight into the impact of IN on colonic Tregs, we performed scRNA-seq to compare the transcriptome of Tregs in the lamina propria of IN-fed and Ctrl-fed mice. To this end, we isolated colonic CD4^{+}Tomato^{+} cells from iFoxp3^{Tomato} mice fed the IN or Ctrl diet after tamoxifen administration 1 day prior to analysis. First, we combined the scRNA-seq data of Tregs in IN-fed and Ctrl-fed mice and identified five clusters (clusters 0–4) in an unbiased manner (Figure S3A). Among four clusters (clusters 0–3) that expressed *Foxp3* (Figures 3A and S3B), the relative abundance of clusters 1 and 3 was dramatically increased in IN-fed mice compared with that in Ctrl-fed mice (Figures 3B and 3C). On the basis of the differentially expressed genes and gene signatures, we identified RORγt^{+} Tregs expressing *Rorc* and *Maf* (cluster 0) and RORγt^{-} Tregs (cluster 1–3) (Figures 3A and 3D). Consistent with previous findings (Miragaia et al., 2019), RORγt^{+} Tregs expressed other Treg signature genes, including *Il10*, *Ctla4*, and *Gzmb* (Figure 3D). *Ikzf2*-positive RORγt^{-} Tregs (Figures 3E and S3B) were further classified into *Gata3*^{hi} tissue-repairing Tregs (“Repair Tregs”) expressing *Gata3* and *Il1rl1* (cluster 2) and *Gata3*^{lo} Tregs (clusters 1 and 3) (Figures 3D and S3B). *Gata3*^{lo} Tregs, which were most abundant in IN-fed mice, consisted of two subsets characterized by the expression of *Gzma* and *Itgae* (genes encoding a cytotoxic granule and αEβ7 integrin, respectively [cluster 1]) and *Itgb1* (a known marker of mobilization [cluster 3]). These findings indicate that the AhR agonist IN induces GATA3^{lo} Helios^{+} Tregs *in vivo* and that these GATA3^{lo} Helios^{+} Tregs display a transcriptomic profile distinct from that of Tregs in Ctrl-fed mice.

Altered localization of colonic Tregs in mice fed the AhR ligand IN

Then we further characterized the AhR agonist IN-induced GATA3^{lo} Helios^{+} Tregs. Using gene ontology (GO) analysis, we searched for biological processes significantly enriched in GATA3^{lo} Helios^{+} Tregs (clusters 1 and 3, dominant RORγt^{-} Treg clusters in IN-fed mice) compared with those in Repair Tregs (cluster 2, a dominant RORγt^{-} Treg cluster in Ctrl diet-fed mice). The GO analysis of GATA3^{lo} Helios^{+} Tregs showed significant enrichment of cytoskeleton- and actin filament-based processes, whereas the GO analysis of Repair Tregs showed significant enrichment of cellular activation, proliferation, and development (Figures S3C and S3D). Therefore, we hypothesized that IN-induced Tregs are highly mobile, similar to Tregs in the small intestine, as we previously reported (Sujino et al., 2016).

We visualized colonic Tregs as Tomato^{+} cells in iFoxp3^{Tomato} mice fed a Ctrl or IN diet using intravital microscopy. As expected, Tomato^{+} cells moved significantly faster in the colon of IN-fed mice than in Ctrl-fed mice (Figures 3F and 3G; Videos S1 and S2). To obtain a detailed view of the location of colonic Tregs, we generated a 3D reconstruction of the colon. Colonic Tregs in Ctrl-fed mice were mainly observed around the bottom of crypts (Figure 3H, upper; Video S3), whereas most Tregs in IN-fed mice were detected close to the top of crypts (Figures 3H, lower, and 3I; Video S4). Moreover, Tregs in IN-fed mice were located close to MHC class II^{+} ECs in the crypt top, and Tregs in Ctrl-fed mice were observed in the crypt bottom. Of note, a low abundance of MHC class II^{+} ECs was detected on the luminal side in Ctrl-fed mice (Figure S3E; Videos S5 and S6). These data suggest that the AhR agonist IN acts on ECs, which subsequently attract Tregs close to the luminal side of the crypts and alter their dynamics *in vivo*. We next examined whether the AhR agonist IN alters the location of Tregs in UC patients, as demonstrated in the mouse model. Given that IN is currently used as a therapeutic agent for UC patients in Asia (Jiang and Cui, 2002; Naganuma et al., 2018), we collected mucosal biopsy

CellPress
OPEN ACCESS

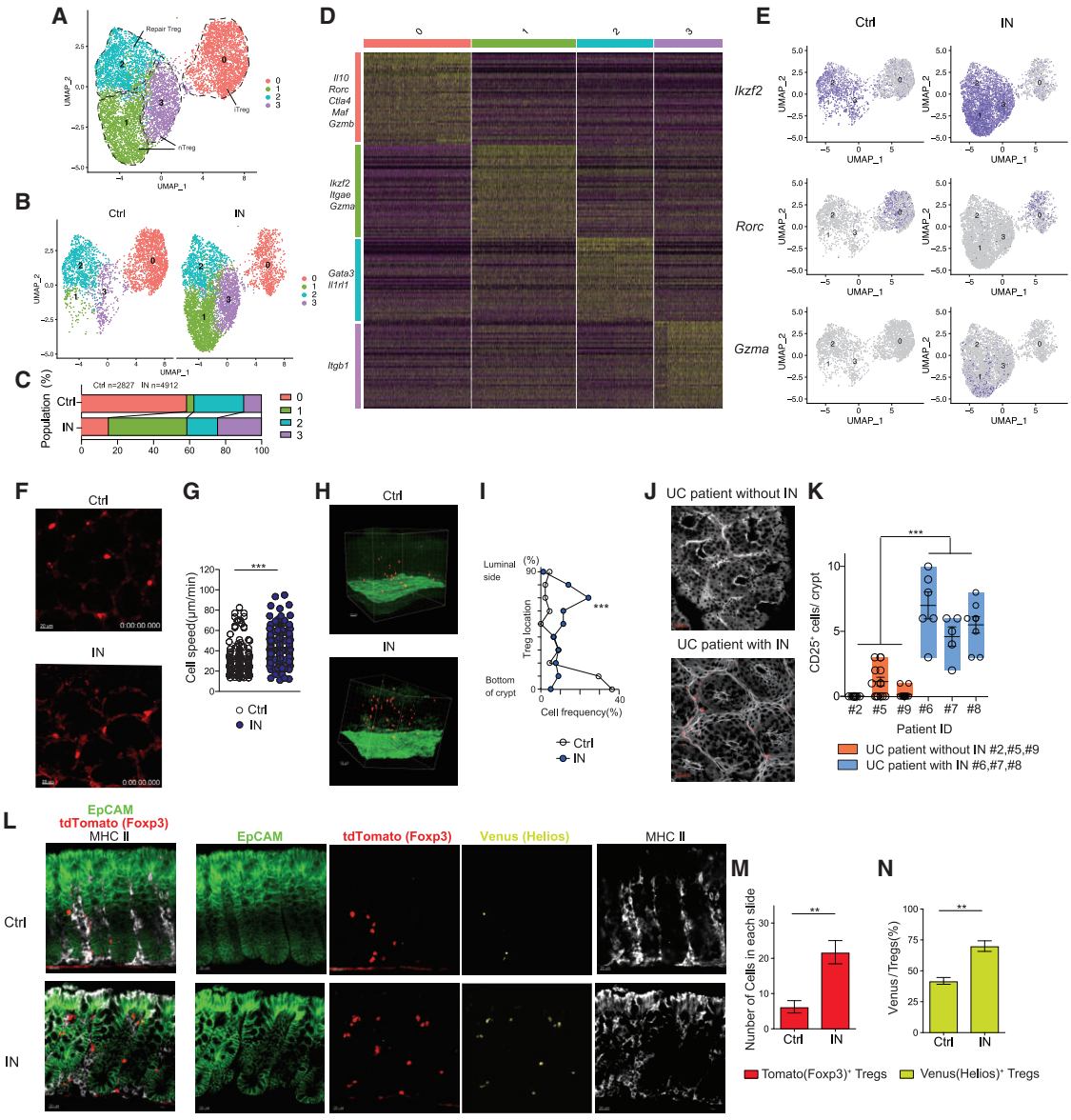

Figure 3. Characteristics of Tregs induced by the AhR agonist IN

(A and B) Uniform manifold approximation and projection (UMAP) representation of sequenced cells, which highly expressed *Foxp3*, color coded by cluster (A), and they were split into each group (B). Cluster names and numbers correspond to colors throughout the figure as indicated.

(C) Population of indicated clusters were calculated based on scRNA-seq data of sequenced cells in each group.

(D) Heatmap of the top differentially genes in Treg cell clusters represented by the normalized *Z* score.

(E) Expression of indicated genes in sequenced cells are shown in UMAP.

(F and G) Intravital microscopy (IVM) analysis of colon crypt obtained from the three independent sites. Time-lapse images of *Helios*^{venus}: *Rosa26*$^{lsl\text{-}tdTomato}$; *Foxp3*$^{eGFP\text{-}Cre\text{-}ERT2}$ mice (red, Foxp3), 24 h after tamoxifen administration for 2 consecutive days (F). The graph shows the average track speed of Treg cells in each colon (G).

(H and I) Reconstructed in 3D imaging (red, Foxp3; green, EpCAM [upper] and second harmonic generation [SHG] [lower]) (H). Frequency of Treg cells (Tomato$^+$ cells obtained from TAM-pretreated *Rosa26*$^{lsl\text{-}tdTomato}$; *Foxp3*$^{eGFP\text{-}Cre\text{-}ERT2}$ mice) location from bottom of crypt to luminal side in the colon of CE2-fed mice and IN-fed mice are shown (I).

(J and K) Representative confocal microscope images of the colon obtained from the three independent sections with or without IN-treated patients (red; CD25) (J) and the number of CD25$^+$ cells of colon crypt in each group are shown (K).

(L–N) Representative colon vibratome section obtained from TAM-pretreated *Helios*^{venus}: *Rosa26*$^{lsl\text{-}tdTomato}$; *Foxp3*$^{eGFP\text{-}Cre\text{-}ERT2}$ mice, which were fed with CE2 diet or IN diet for 3 weeks, were imaged with two-photon microscopy (yellow, Helios; red, Foxp3; white, MHC classII; green, EpCAM). Images are obtained from three independent sites and captured by overlay (L, each left side) and single (L, each right side) channel. Number of Tomato (Foxp3)$^+$ cells (M) and Venus (Helios)$^+$ (N) are counted in each four fields of view. p values obtained via by Student's t test (G, M, and N), Mann Whitney U test (I), ANOVA with post Boneferroni's multiple compare test (K). **<0.01, ***<0.001. ns: not significant. Data are shown as mean ± SD (I and K) or ± SE (G, M, and N) of individual cells, and they are representative of two independent experiments (G, I, M, and N).

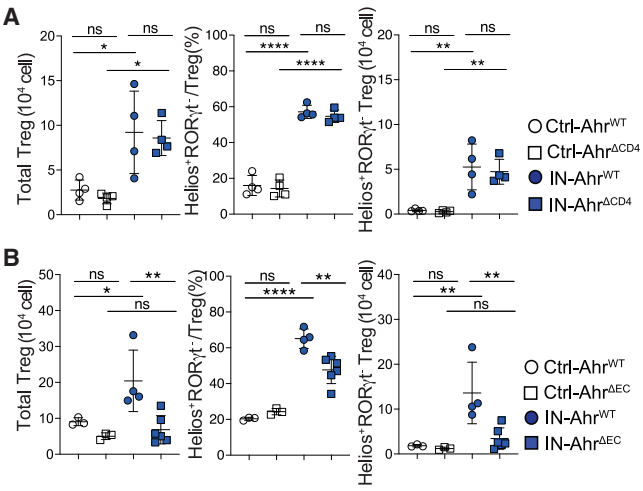

Figure 4. AhR signaling in the epithelial cells is indispensable for increase of Helios$^+$ RORγt$^-$ Tregs

(A) *Cd4*$^{Cre\text{-}ERT2}$:*Ahr* $^{fl/fl}$ mice were treated with corn oil (AhR^{WT} mice) or TAM administration (AhR$^{\Delta CD4}$ mice) for total of 4 days, followed by receiving CE2 diet (Ctrl) or CE2 with 4% IN (IN) for 3 weeks (n = 4/group). Percentage of Helios$^+$ RORγt$^-$ cells among Tregs in cLP, number of Tregs and Helios$^+$ RORγt$^-$ Tregs are shown.

(B) *villin*$^{Cre\text{-}ERT2}$:*Ahr*$^{fl/fl}$ mice were treated with corn oil (AhR^{WT} mice) or TAM administration (AhR$^{\Delta EC}$ mice) for total of 4 days followed by receiving Ctrl diet or IN diet for 3 weeks (n = 4–6/group). Percentage of Helios$^+$ RORγt$^-$ cells among Tregs in cLP, number of Tregs and Helios$^+$ RORγt$^-$ Tregs are shown. p values obtained via by one-way ANOVA with Tukey's post hoc test. *<0.05, **<0.01, ****<0.0001. ns: not significant. Data are shown as mean ± SD of individual mice (n = 4–6), representative of two independent experiments.

samples from the colon of UC patients treated with or without IN therapy. UC patients who received IN therapy showed an increased number of Tregs (defined as CD25$^+$ cells) near the top of crypts compared with those who were not administered IN therapy (Figures 3J and 3K), supporting our hypothesis that IN induces the accumulation of Tregs near the crypt top in both mice and UC patients.

Given that Tregs in IN-fed mice expressed high levels of CD103 (Figures 2F and 3D), which forms a heterodimer with integrin β7 and binds to E-cadherin in the gut (Cepek et al., 1994; Pauls et al., 2001), we considered the possibility of a potential interaction between Tregs and intestinal ECs in the gut. Indeed, a recent report showed that Tregs interact with epithelial stem cells through MHC class II molecules to maintain intestinal homeostasis (Biton et al., 2018). Therefore, we performed immunohistological staining of EpCAM and MHC class II using colon tissue samples from *Helios*^{Venus}:i*Foxp3*^{Tomato} mice and visualized the location of Tregs in the colon. In Ctrl-fed mice, most Tomato$^+$ Tregs were observed around the bottom of crypts (Figure 3L). In contrast, total (Tomato$^+$) and Helios$^+$ (Tomato$^+$Venus$^+$) Tregs were significantly increased and located near the luminal side in IN-fed mice (Figures 3L–3N). Interestingly, unlike the ubiquitous expression of EpCAM, the expression of MHC class II was restricted to ECs on the luminal side in IN-fed mice compared with that in Ctrl-fed mice (Figure 3L). Therefore, we considered the possibility that IN induces antigen-specific Tregs. We challenged ovalbumin (OVA)-specific TCR transgenic mice of a *Rag2*$^{-/-}$ background (*Rag2*$^{-/-}$:OT-II) with OVA and the IN or Ctrl diet. The total number of Tregs and proportion of Helios$^+$ RORγt$^-$ and Helios$^-$ RORγt$^+$ Tregs were comparable between *Rag2*$^{-/-}$:OT-II mice fed OVA and the IN diet or Ctrl diet (Figure S3F), suggesting that IN does not preferentially induce antigen-specific Tregs. Consistently, scRNA/TCR-seq revealed that the proportion of Tregs (clusters 0–3 in Figures 3A–3C) with a relatively large clone size (defined as more than 1%) was less than 10% in both IN-fed mice and Ctrl-fed mice (Figure S3G), and the TCR clones of each cluster were more diverse in IN-fed mice than in Ctrl-fed mice (Figure S3H). No increases in the total number of Tregs or the percentage of Helios$^+$ RORγt$^-$ Tregs were observed in germ-free (GF) mice fed a sterile IN diet (Figure S3I), suggesting that the induction of colonic Tregs by IN depends on commensal bacteria. We also found that the microbiome composition was altered in IN-fed mice (Figures S3J–S3L); however, previous reports indicate that the microbiome induces RORγt$^+$ Tregs (Atarashi et al., 2011; Nutsch et al., 2016; Sakaguchi et al., 2008; Sefik et al., 2015). Moreover, anti-microbiome treatment (ampicillin, metronidazole, neomycin sulfate, or vancomycin) did not inhibit the accumulation of Helios$^+$ RORγt$^-$ Tregs under the IN diet, indicating that a specific microbiome is not essential for IN-induced Tregs (Figures S3M and S3N). Collectively, these data indicate that IN induces polyclonal Helios$^+$ RORγt$^-$ Tregs in the presence of commensal intestinal bacteria.

AhR signals in ECs are essential for IN-induced accumulation of Tregs in the colon

To identify the potential molecular mechanisms underlying the IN-induced accumulation of Tregs in the colon, we next investigated the types of cells that primarily respond to the AhR ligand IN. The AhR is a ligand-dependent transcription factor that regulates several genes in response to environmental cues (Mezrich et al., 2010; Quintana et al., 2010). AhR signaling has been reported to maintain intestinal homeostasis by directly altering the transcriptional program of Tregs and ECs (Quintana et al., 2008; Schiering et al., 2017). Therefore, we analyzed the T cell- and EC-specific effects of AhR signaling on colonic Treg accumulation in *Ahr*$^{f/f}$, *Cd4*$^{Cre\text{-}ERT2}$:*Ahr*$^{f/f}$, and *Villin*$^{Cre\text{-}ERT2}$:*Ahr*$^{f/f}$ mice (referred to as AhR^{WT}, AhR$^{\Delta CD4}$, and AhR$^{\Delta EC}$, respectively) treated with tamoxifen and fed the IN diet for 3 weeks. AhR^{WT} mice fed the IN diet (IN-AhR^{WT}) and AhR$^{\Delta CD4}$ mice fed the IN diet (IN-AhR$^{\Delta CD4}$) showed a similar significant increase in the number of Helios$^+$ RORγt$^-$ Tregs (Figures 4A and S4A). Interestingly, the number of Helios$^+$ RORγt$^-$ Tregs was significantly lower in AhR$^{\Delta EC}$ mice fed the IN diet (IN-AhR$^{\Delta EC}$) than in IN-AhR^{WT} (Figures 4B and S4B). In addition, CD103 expression in Tregs was reduced to basal levels in IN-AhR$^{\Delta EC}$ mice (Figure S4C). These findings indicate that AhR signaling in ECs but not Tregs is critical for the accumulation of Helios$^+$ RORγt$^-$ Tregs in the colon of IN-fed mice.

To identify the potential molecular mechanisms by which AhR signaling in ECs contributes to the increase in colonic Tregs in IN-fed mice, we performed RNA-seq to compare ECs in WT mice fed the Ctrl or IN diet (Ctrl-AhR^{WT} and IN-AhR^{WT}, respectively) and IN-AhR$^{\Delta EC}$. Unbiased hierarchical clustering of transcriptomes in these three groups revealed that the transcriptome of ECs in IN-AhR^{WT} mice was clearly distinct from that in Ctrl-AhR^{WT} and

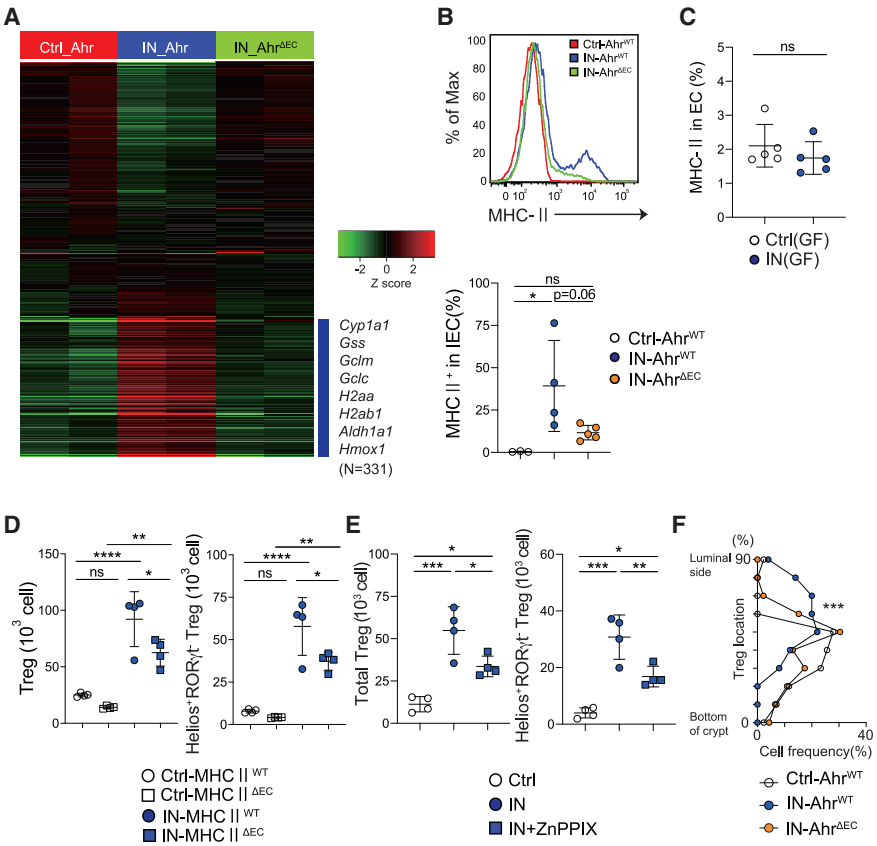

Figure 5. MHC class II molecules and heme oxygenase induced by AhR signaling of ECs are important for Helios$^+$ RORγt$^-$ Tregs accumulation in the colon

(A) Heatmap of the top differentially expressed genes of classified by sorted colon epithelial cells (ECs) of Ctrl-AhR^{WT}, IN-AhR^{WT}, and IN-AhR$^{\Delta EC}$ mice. Representative gene name is listed on the right.

(B) Representative FACS plot and percentage of MHC classII$^+$ cells among CD45$^-$EpCAM$^+$EC are shown.

(C) Germ-free mice receiving sterile Ctrl diet or IN diet for 3 weeks (n = 5/group) were analyzed. Percentage of MHC classII$^+$ cells among CD45$^-$EpCAM$^+$EC are shown.

(D) *villin*$^{Cre\text{-}ERT2}$:*h2ab1*$^{fl/fl}$ mice were treated with corn oil (MHCII^{WT} mice) or TAM administration (MHCII$^{\Delta EC}$ mice) for total of 4 days, followed by receiving Ctrl diet or 4% IN diet for 3 weeks (n = 4/group) and analyzed. Bar graph shows number of Tregs and Helios$^+$ RORγt$^-$ Tregs in cLP.

(E) 7-week-old C57BL/6J mice fed with Ctrl diet (Ctrl) or 4% IN diet for 3 weeks. Half of IN diet mice were treated with zinc protoporphyrin-9 (ZnPPIX) (IN + ZnPPIX) and the latter half of IN diet mice were treated with mixture of dimethyl sulfoxide (DMSO) and PBS as control (IN).

(F) The percentage of CD25$^+$ cells location from bottom of crypt to luminal side in the colon of Ctrl-AhR^{WT}, IN-AhR^{WT}, and IN-AhR$^{\Delta EC}$ mice. p values obtained via by one-way ANOVA with Tukey's post hoc test (B and D–E), Student's t test (C), and Mann Whitney U test (F).*<0.05, **<0.01, ***<0.001,****<0.0001. ns: not significant. Data are shown as mean ± SD of individual mice (n = 4–5), representative of two independent experiments.

IN-AhR$^{\Delta EC}$ mice (Figure S5A). This suggests that IN-AhR signaling is a major determinant of transcriptomic changes in ECs, although a mixture of known representative ingredients in IN, AhR ligands (including indigo, indirubin, and anthranilic acid), and betulin was not sufficient to increase colonic Tregs (Figure S5B). Among 331 genes significantly upregulated in the ECs of IN-AhR^{WT} mice compared with those in Ctrl-AhR^{WT} and IN-AhR$^{\Delta EC}$ mice, we further verified the expression of MHC class II-related genes (*H2aa and H2ab1*) in the ECs of IN-AhR^{WT} mice (Figure 5A). As shown in Figure 3L, IN-AhR^{WT} mice displayed a higher percentage of MHC class II$^+$ ECs than Ctrl-AhR^{WT} mice, which was not observed in IN-AhR$^{\Delta EC}$ mice (Figure 5B). We also confirmed that GF mice fed a sterile IN diet did not exhibit increased MHC class II expression on ECs, which is consistent with the data that a sterile IN diet does not increase Helios$^+$RORγt$^-$Tregs in GF mice (Figures 5C and S3I). These findings indicate that both gut microbiota and AhR ligands are indispensable for MHC class II expression in colonic ECs. To uncover the involvement of MHC class II signals in ECs in the induction of IN-Tregs, we generated a genetic model of MHC class II deletion in ECs (*H2ab1*$^{f/f}$ [MHC II^{WT}] and *Villin*$^{Cre\text{-}ERT2}$:*h2ab1*$^{f/f}$ [MHC II$^{\Delta EC}$] mice) fed with or without the IN diet (referred to as Ctrl-MHC II^{WT}, Ctrl-MHC II$^{\Delta EC}$, IN-MHC II^{WT}, and IN-MHC II$^{\Delta EC}$) (Figures S5C and S5D). The number and percentage of Helios$^+$ Tregs were slightly but significantly lower in IN-MHC II$^{\Delta EC}$ mice than in IN-MHC II^{WT} mice. Of note, Helios$^+$ Tregs in IN-MHC II$^{\Delta EC}$ mice were still increased compared with those in Ctrl-MHC II$^{\Delta EC}$ mice (Figure 5D). These data indicate that MHC II expression on ECs is partially involved in the induction of IN-Tregs. In addition, GO analysis showed enrichment of genes related to systemic processes (*Hmox1*, a heme oxygenase-related gene), glutathione metabolic and cofactor metabolic pathways (*Gss*, *Gclm, Gclc, Aldh1a1*), and responses to xenobiotic stimuli (*Cyp1a1*, an AhR-targeted gene) (Figures 5A and S5E). Therefore, we next evaluated the effect of a heme oxygenase inhibitor on colonic Tregs in IN-fed mice and observed that zinc protoporphyrin-9 significantly reduced total and Helios$^+$RORγt$^-$ Tregs in IN diet-fed mice (Figure 5E). Although glutathione metabolic process-related genes were enriched in the ECs of IN-MHC II^{WT} mice (Figures S5E and S5F), the administration of the glutathione inhibitor buthionine sulfoximine did not reduce the total number of Helios$^+$RORγt$^-$ Tregs in IN-fed mice (Figure S5G). These data indicate that MHC class II and heme oxygenase expression induced by IN through AhRs in ECs are important for IN-Treg accumulation in the colon. Lastly, we investigated whether IN-AhR signaling in ECs determines the localization of IN-Tregs in the gut. We generated a 3D histological construction of colonic specimens and determined the location of CD25$^+$ cells in the crypt bottom in Ctrl-AhR^{WT}, IN-AhR^{WT}, and IN-AhR$^{\Delta EC}$ mice. As expected, the location of CD25$^+$ cells was significantly

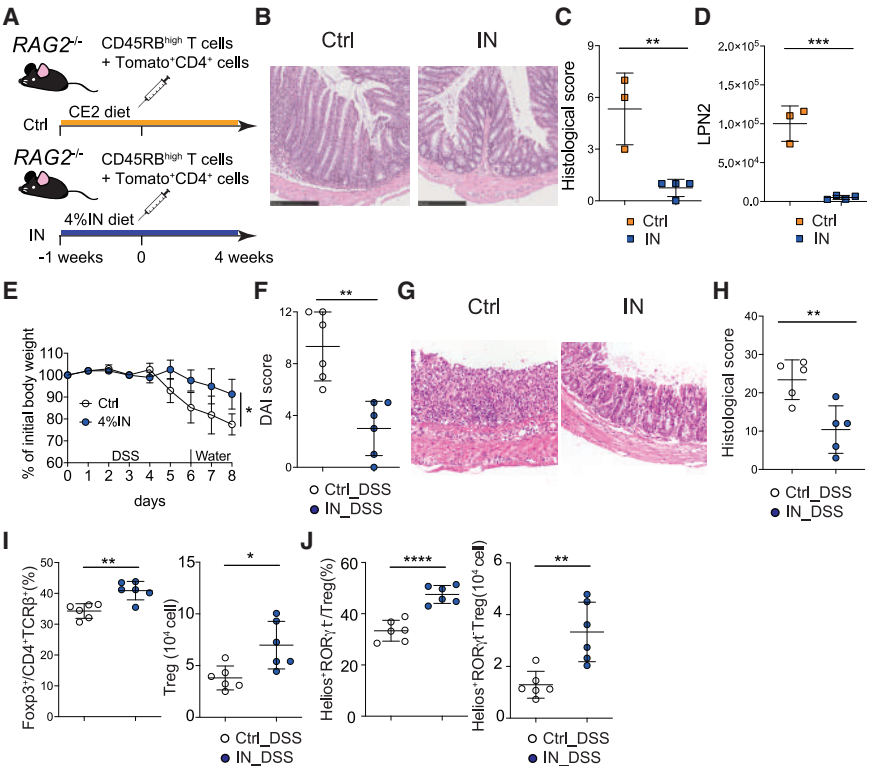

Figure 6. IN diet ameliorates colitis with the increase in number of Helios$^+$ RORγt$^-$ Tregs

(A–D) *RAG2* $^{-/-}$ mice were transferred with Ly5.1$^+$CD4$^+$CD45RB^{high} T cells plus tdTomato$^+$ CD4$^+$ T cells of spleen and mesenteric lymph node obtained from *Rosa26*$^{lsl\text{-}tdTomato}$; *Foxp3*$^{eGFP\text{-}Cre\text{-}ERT2}$ mice, which were treated with TAM administration for consecutive 2 days, followed by receiving Ctrl diet or IN diet for 3 weeks (A). Representative H&E stained histological sections from colon (B), histological scores (C), and fecal lipocalin-2 (D) in the fourth week after transfer are shown.

(E–J) C57BL/6J mice of 7 weeks received CE2 diet (Ctrl) or CE2 with 4% indigo naturalis (IN) for 3 weeks (n = 6/group); then mice were treated with 2% DSS in drinking water. Body weight change (E), DAI score (F), representative H&E stained histological sections from colon (G), and histological scores (H) are shown. Percentage of Tregs among CD4$^+$TCRβ$^+$ lymphocyte subsets, number of Tregs (I), percentage of Helios$^+$ RORγt$^-$ cells among Treg cell subsets, and number of Tregs (J) are shown. p values obtained via by Student's t test. *<0.05, **<0.01, ***<0.001, ****<0.0001. ns: not significant. Data are shown as mean ± SD of individual mice (n = 3–6), representative of two independent experiments.

shifted toward the luminal side in IN-AhR^{WT} mice compared with that in IN-AhR$^{\Delta EC}$ and Ctrl-AhR^{WT} mice (Figure 5F). Thus, these findings suggest that IN-AhR signaling in ECs governs the accumulation and localization of IN-Tregs in the gut.

IN diet ameliorates experimental colitis

Given that IN did not promote the differentiation of Tregs from naive T cells, we aimed to determine the effect of IN on Tregs in colitis. To this end, we analyzed *Rag2*$^{-/-}$ mice implanted with naive T cells (CD4$^+$CD45RB^{high} cells from WT mice) and Tregs (CD4$^+$TCRβ$^+$Tomato$^+$ cells from iFoxp3^{Tomato} mice) at a ratio of 8:1 (Figure 6A). Consistent with previous reports (Powrie et al., 1993), Ctrl-diet *Rag2*$^{-/-}$ mice implanted with naive T cells and Tregs developed colitis due to the low number of co-transferred Tregs. However, IN supplementation significantly ameliorated colitis (Figures 6B–6D). IN-fed *Rag2*$^{-/-}$ mice inoculated with naive T cells and Tregs showed reductions in Th1 cells (Figure S6A), which are a critical immune subset for colonic inflammation and weight loss (Sujino et al., 2011). In addition to adoptive transfer colitis, the IN diet ameliorated dextran sodium sulfate (DSS)-induced colitis compared with the Ctrl diet (Figures 6E–6H). Of note, we observed an increased number of Helios$^+$RORγt$^-$Tregs in IN-fed mice, whereas Helios$^-$RORγt$^+$ Tregs or other immune cell subsets were unaffected (Figures 6I and 6J and S6B–S6E). In addition, the IN diet did not suppress colitis in *Rag2*$^{-/-}$ mice in the absence of Tregs, suggesting that IN-mediated anti-colitic effects are T cell dependent (Figures S6F and S6G). Colonic Tregs obtained from IN-fed mice were functional and suppressed the proliferation of naive T cells under CD3/CD28 stimulation, similar to those from Ctrl-fed mice (Figure S6H). Collectively, these data suggest that IN exerted an anti-inflammatory function *in vivo* through increasing Tregs in the gut.

DISCUSSION

Tregs play a pivotal role in controlling excessive inflammation in the colon, and there is increasing interest in developing Treg therapies to treat IBD and autoimmune diseases. Here, we demonstrated that IN, a phytochemical AhR-agonist-containing compound, increased the number of Tregs predominantly in the colon near the crypt top. These Tregs induced by the AhR ligand were characterized by GATA3^{lo} Helios$^+$ RORγt$^-$ and possessed a specific gene expression profile, such as *Gzma* and *Prf1*. The accumulation of colonic Tregs in IN-fed mice near the crypt top of the lamina propria was dependent on IN-AhR signaling in ECs but not T cells. In addition, conditional deletion of MHC class II genes and chemical perturbation of heme oxygenase in ECs reduced the total number of Tregs. Accordingly, IN treatment increased the number of Tregs and ameliorated the severity of a DSS-induced colitis model.

To date, several researchers have attempted to increase the number of Tregs and enhance their function in patients with autoimmune diseases and IBD (Clough et al., 2020; Raffin et al., 2020). However, there is limited evidence describing the efficacy of the adoptive transfer of Tregs, except for some clinical studies with a small number of patients (Brunstein et al., 2016; Desreumaux et al., 2012). This might be attributed to the difficulty in obtaining stable Foxp3 expression and gut-homing ability in human Tregs.

Instead of transferring Tregs, their expansion or recruitment in the gut is an alternative strategy for treating IBD, and the AhR has become an attractive therapeutic target (Gutiérrez-Vázquez and Quintana, 2018). Indeed, we and another group reported that IN or other nontoxic AhR agonists ameliorate colitis in both human and mouse models (Goettel et al., 2016; Kawai et al., 2017; Naganuma et al., 2018; Sugimoto et al., 2016b; Yoshimatsu et al., 2020). Our data added mechanistic insight into the regulatory mechanisms that induce a tolerogenic environment in the gut.

Previous studies elucidated the effects of AhR signaling on pTregs (Brandstätter et al., 2016; Gandhi et al., 2010; Goettel et al., 2016; Mezrich et al., 2010; Monteleone et al., 2011; Qiu et al., 2012), and our investigation of a phytochemical AhR agonist revealed several important aspects of the mechanisms underlying intestinal homeostasis and pathology. IN treatment increased the number of Tregs by priming ECs to express MHC class II molecules. Lgr5^{+} intestinal stem cells and ECs express MHC class II molecules and induce IL-10^{+} Tregs or Helios^{-} Tregs in the small intestine, respectively (Biton et al., 2018; Stephens et al., 2021). We showed that a small number of colonic ECs express MHC class II molecules in the steady state, and IN increases Tregs via enhancing MHC class II expression in colonic ECs. Our observation that a lack of AhRs in ECs resulted in a slight reduction in the total number of Tregs but not Helios^{+} Tregs under the Ctrl diet suggests that AhR signaling in ECs maintains pTregs through MHC class II expression in the steady state.

scRNA-seq data revealed that Tregs in IN-fed mice mainly comprised GATA3^{lo}Helios^{+} Tregs expressing *Gzma* and *Prf1*, which are effector molecules of Tregs (Cao et al., 2007; Grossman et al., 2004) and cytotoxic T lymphocytes (Voskoboinik et al., 2015). Further studies are needed to determine the precise mechanism and role of effector molecules in IN-Tregs in the gut. This specific feature of IN-induced Tregs provides mechanistic insight into the roles of AhR agonists in controlling intestinal inflammation.

Multiple local environmental factors contribute to the development and maintenance of intestinal Tregs, including gut microbiota and food antigens (Miragaia et al., 2019; Tanoue et al., 2016; Whibley et al., 2019). However, several tTregs are observed in the colon and respond to microbial antigens, although tTregs have been thought to be selected in the thymus by self-antigens (Littman and Rudensky, 2010; Ohkura et al., 2013; Sakaguchi et al., 2008). Some tTregs are possibly selected by microbial antigens presented on thymic ECs and recognize microbial antigens in the colon (Zegarra-Ruiz et al., 2021). In addition, Helios^{+} Tregs are generally recognized as thymic-derived Tregs, but pTregs or inducible Tregs express Helios in some *in vitro* settings (Akimova et al., 2011; Gottschalk et al., 2012). The polyclonality of the TCR repertoire appears to be important for Tregs to express Helios and maintain immunological homeostasis in the intestine (Nishio et al., 2015; Thornton et al., 2010). We observed a variety of TCR clonotypes in colonic IN-Tregs, suggesting that IN did not increase antigen-specific Tregs. The original IN-Tregs and TCR antigens, along with the involvement of microbiota, remain of interest for future exploration.

We demonstrate that IN-Tregs express not only effector molecules but also CD103. CD103 is expressed by Tregs with a suppressive capacity following activation (Annacker et al., 2005; Lehmann et al., 2002; McHugh et al., 2002) and is required for Treg localization (Schön et al., 1999; Suffia et al., 2005). We showed that IN-induced Tregs localize near the top of the crypt in the colon, and some Tregs reside next to MHC II^{+} ECs. Moreover, the localization of CD25^{+} cells near the crypt top was observed in UC patients treated with AhR agonists, despite some contamination from activated non-Tregs. A small proportion of Helios^{+} Tregs may migrate from the lamina propria to the intraepithelial compartment, as observed in the small intestine (Morikawa et al., 2021; Sujino et al., 2016). However, because of the sparseness of intraepithelial lymphocytes (Harada et al., 2022; London et al., 2021; Sujino et al., 2016), the roles of CD103 in IN-induced Tregs and their localization near the top of the crypts or intraepithelial space remain to be elucidated. This dynamic process is mainly dependent on AhR signaling in ECs but not T cells because the total number and location of Tregs in mice with EC-specific deletion of *AhR* were similar to those observed in Ctrl-fed mice.

Overall, we identified that the activation of AhR signaling in ECs induced the accumulation of Helios^{+} Tregs, which expressed genes related to cytotoxic functions, including *Gzma* and *Prf1*. In addition, AhR-signaling activation changed the localization of intestinal Tregs in the gut near the luminal side. Understanding the physiological roles and localization of Tregs in the intestine and other peripheral tissues may lead to a breakthrough in therapeutic strategies for autoimmune diseases, infection, and cancer. Our data provide convincing mechanistic insight, highlighting the potential use of nontoxic AhR agonists for treatment of IBD.

Limitations of the study

We obtained samples from only three patients with UC in each treatment group because of the limited number of patients receiving IN. In addition, it is well known that CD25-negative Tregs are present in the intestine. However, Foxp3-positive cells in humans, including non-suppressive activated cells, are also functionally and phenotypically heterogeneous (Miyara et al., 2009; Sakaguchi et al., 2010; Sugiyama et al., 2013). Therefore, we showed CD25-positive cells as the suppressive cells. Regarding AhR signals in the intestinal epithelium, the increased rate of Helios^{+} Tregs induced by IN was not completely prevented in IN-AhR$^{\Delta EC}$ mice. This finding indicates that another mechanism possibly contributes to the accumulation of IN-induced Tregs. The AhR ligand IN contains a mixture of AhR ligands, such as indigo and indirubin. Therefore, the single substance that increases IN-Tregs remains unknown. Moreover, the cells suppressed by cytotoxic cells, such as IN-Tregs, remain to be identified. Given that Tregs have a variety of suppressive functions, further analysis of the interactions between cytotoxic cells, including IN-Tregs, and other target cells is required.

STAR★METHODS

Detailed methods are provided in the online version of this paper and include the following:

- KEY RESOURCES TABLE
- RESOURCE AVAILABILITY
  - Lead contact
  - Materials availability

SUPPLEMENTAL INFORMATION

Supplemental information can be found online at https://doi.org/10.1016/j.celrep.2022.110773.

ACKNOWLEDGMENTS

We thank Chiemi Ido, Ena Nomura, Yuzo Koda, Hiroki Kiyohara, Nobuhito Taniki, Koji Okabayashi (Keio University), Daniel Mucida (The Rockefeller University), Mariya London (New York University), Shohei Hori (Tokyo University), Takatoshi Chinen (Kyushu University), and Tsudoi Miyamoto for their discussion and reading of the manuscript and the JKic, Keio core facility for helping with multi-photon microscopy. We thank Melissa Crawford, PhD, from Edanz (https://jp.edanz.com/ac) for editing a draft of this manuscript. Grants-in-Aid from the Japanese Society for the Promotion of Science (JSPS) (17K19668, 17H05082, 19K22624, 20H03665, 21K18272 to T.S., 21K07084 to K.O., 19K08402 to N.H., 21H02905 to H.O., 20H00536 to T.K., 17H06175 and JP21H05044 to A.Y.), The Japan Agency for Medical Research and Development (19ek0109214 to T.S. and CREST-16813798, 21gm1510002h0001 to T.K., CREST-1110009, CREST JP21gm1110009, and MOON SHOT JP21zf0127003h to A.Y.), The Yakult Bioscience Research Foundation (T.S.), The Keio University Medical Science Fund (Sakaguchi Memorial, Fukuzawa Memorial) (T.S.), The Takeda Science Foundation, the Mochida Memorial Foundation (T.S.), GSK Science Foundation (T.S.), JSR Research Fund (T.S.), Mitsubishi Foundation (T.K.), and Princess Takamatsu Cancer Research Foundation, Yasuda Medical Foundation (A.Y.).

AUTHOR CONTRIBUTIONS

Conceptualization: Y.Y. and T.S.; methodology: Y.Y., K.M., T.S., Y.H., S.T., K.O., S.U., K.Y., T.T., T.S., N.S., K.T., K.S., and T.I.; investigation: Y.Y., K.M., T.S., Y.H., and N.S.; visualization: Y.Y., K.M., T.S., Y.H., and N.S.; funding acquisition: T.S., N.H., H.O., A.Y., and T.K.; project administration: T.S.; supervision: T.S. and T.K.; writing – original draft: Y.Y. and T.S.; and writing – review & editing: K.M., Y.Y., Y.M., N.N., A.Y., and T.K.

DECLARATION OF INTERESTS

K.M. and T.S. are employees of Miyarisan Pharmaceutical Co., Ltd.

Received: June 1, 2021
Revised: December 30, 2021
Accepted: April 12, 2022
Published: May 10, 2022

REFERENCES

Akimova, T., Beier, U.H., Wang, L., Levine, M.H., and Hancock, W.W. (2011). Helios expression is a marker of T cell activation and proliferation. PLoS One *6*, e24226. https://doi.org/10.1371/journal.pone.0024226.

Amiya, T., Nakamoto, N., Chu, P.S., Teratani, T., Nakajima, H., Fukuchi, Y., Taniki, N., Yamaguchi, A., Shiba, S., Miyake, R., et al. (2016). Bone marrow-derived macrophages distinct from tissue-resident macrophages play a pivotal role in Concanavalin A-induced murine liver injury via CCR9 axis. Sci. Rep. *6*, 35146. https://doi.org/10.1038/srep35146.

Annacker, O., Coombes, J.L., Malmstrom, V., Uhlig, H.H., Bourne, T., Johansson-Lindbom, B., Agace, W.W., Parker, C.M., and Powrie, F. (2005). Essential role for CD103 in the T cell-mediated regulation of experimental colitis. J. Exp. Med. *202*, 1051–1061. https://doi.org/10.1084/jem.20040662.

Atarashi, K., Tanoue, T., Shima, T., Imaoka, A., Kuwahara, T., Momose, Y., Cheng, G., Yamasaki, S., Saito, T., Ohba, Y., et al. (2011). Induction of colonic regulatory T cells by indigenous Clostridium species. Science *331*, 337–341. https://doi.org/10.1126/science.1198469.

Belkaid, Y., and Hand, T.W. (2014). Role of the microbiota in immunity and inflammation. Cell *157*, 121–141. https://doi.org/10.1016/j.cell.2014.03.011.

Biton, M., Haber, A.L., Rogel, N., Burgin, G., Beyaz, S., Schnell, A., Ashenberg, O., Su, C.W., Smillie, C., Shekhar, K., et al. (2018). T helper cell cytokines modulate intestinal stem cell renewal and differentiation. Cell *175*, 1307–1320.e22. https://doi.org/10.1016/j.cell.2018.10.008.

Brandstätter, O., Schanz, O., Vorac, J., König, J., Mori, T., Maruyama, T., Korkowski, M., Haarmann-Stemmann, T., von Smolinski, D., Schultze, J.L., et al. (2016). Balancing intestinal and systemic inflammation through cell type-specific expression of the aryl hydrocarbon receptor repressor. Sci. Rep. *6*, 26091. https://doi.org/10.1038/srep26091.

Brunkow, M.E., Jeffery, E.W., Hjerrild, K.A., Paeper, B., Clark, L.B., Yasayko, S.A., Wilkinson, J.E., Galas, D., Ziegler, S.F., and Ramsdell, F. (2001). Disruption of a new forkhead/winged-helix protein, scurfin, results in the fatal lymphoproliferative disorder of the scurfy mouse. Nat. Genet. *27*, 68–73. https://doi.org/10.1038/83784.

Brunstein, C.G., Miller, J.S., McKenna, D.H., Hippen, K.L., DeFor, T.E., Sumstad, D., Curtsinger, J., Verneris, M.R., MacMillan, M.L., Levine, B.L., et al. (2016). Umbilical cord blood-derived T regulatory cells to prevent GVHD: kinetics, toxicity profile, and clinical effect. Blood *127*, 1044–1051. https://doi.org/10.1182/blood-2015-06-653667.

Campos-Mora, M., Contreras-Kallens, P., Gálvez-Jirón, F., Rojas, M., Rojas, C., Refisch, A., Cerda, O., and Pino-Lagos, K. (2019). CD4+Foxp3+T regulatory cells promote transplantation tolerance by modulating effector CD4+ T cells in a neuropilin-1-dependent manner. Front. Immunol. *10*, 882. https://doi.org/10.3389/fimmu.2019.00882.

Cao, X., Cai, S.F., Fehniger, T.A., Song, J., Collins, L.I., Piwnica-Worms, D.R., and Ley, T.J. (2007). Granzyme B and perforin are important for regulatory T cell-mediated suppression of tumor clearance. Immunity *27*, 635–646. https://doi.org/10.1016/j.immuni.2007.08.014.

Cepek, K.L., Shaw, S.K., Parker, C.M., Russell, G.J., Morrow, J.S., Rimm, D.L., and Brenner, M.B. (1994). Adhesion between epithelial cells and T lymphocytes mediated by E-cadherin and the alpha E beta 7 integrin. Nature *372*, 190–193. https://doi.org/10.1038/372190a0.

Chassaing, B., Srinivasan, G., Delgado, M.A., Young, A.N., Gewirtz, A.T., and Vijay-Kumar, M. (2012). Fecal lipocalin 2, a sensitive and broadly dynamic

non-invasive biomarker for intestinal inflammation. PLoS One *7*, e44328. https://doi.org/10.1371/journal.pone.0044328.

Clough, J.N., Omer, O.S., Tasker, S., Lord, G.M., and Irving, P.M. (2020). Regulatory T-cell therapy in Crohn's disease: challenges and advances. Gut *69*, 942–952. https://doi.org/10.1136/gutjnl-2019-319850.

Desreumaux, P., Foussat, A., Allez, M., Beaugerie, L., Hébuterne, X., Bouhnik, Y., Nachury, M., Brun, V., Bastian, H., Belmonte, N., et al. (2012). Safety and efficacy of antigen-specific regulatory T-cell therapy for patients with refractory Crohn's disease. Gastroenterology *143*, 1207–1217.e2. https://doi.org/10.1053/j.gastro.2012.07.116.

Gandhi, R., Kumar, D., Burns, E.J., Nadeau, M., Dake, B., Laroni, A., Kozoriz, D., Weiner, H.L., and Quintana, F.J. (2010). Activation of the aryl hydrocarbon receptor induces human type 1 regulatory T cell-like and Foxp3(+) regulatory T cells. Nat. Immunol. *11*, 846–853. https://doi.org/10.1038/ni.1915.

Goettel, J.A., Gandhi, R., Kenison, J.E., Yeste, A., Murugaiyan, G., Sambanthamoorthy, S., Griffith, A.E., Patel, B., Shouval, D.S., Weiner, H.L., et al. (2016). AHR activation is protective against colitis driven by T cells in humanized mice. Cell Rep. *17*, 1318–1329. https://doi.org/10.1016/j.celrep.2016.09.082.

Gottschalk, R.A., Corse, E., and Allison, J.P. (2012). Expression of Helios in peripherally induced Foxp3+ regulatory T cells. J. Immunol. *188*, 976–980. https://doi.org/10.4049/jimmunol.1102964.

Grossman, W.J., Verbsky, J.W., Barchet, W., Colonna, M., Atkinson, J.P., and Ley, T.J. (2004). Human T regulatory cells can use the perforin pathway to cause autologous target cell death. Immunity *21*, 589–601. https://doi.org/10.1016/j.immuni.2004.09.002.

Gruber, M., Hu, C.J., Johnson, R.S., Brown, E.J., Keith, B., and Simon, M.C. (2007). Acute postnatal ablation of Hif-2alpha results in anemia. Proc. Natl. Acad. Sci. U.S.A. *104*, 2301–2306. https://doi.org/10.1073/pnas.0608382104.

Gutiérrez-Vázquez, C., and Quintana, F.J. (2018). Regulation of the immune response by the aryl hydrocarbon receptor. Immunity *48*, 19–33. https://doi.org/10.1016/j.immuni.2017.12.012.

Harada, Y., Sujino, T., Miyamoto, K., Nomura, E., Yoshimatsu, Y., Tanemoto, S., Umeda, S., Ono, K., Mikami, Y., Nakamoto, N., et al. (2022). Intracellular metabolic adaptation of intraepithelial CD4(+)CD8αα(+) T lymphocytes. iScience *25*, 104021. https://doi.org/10.1016/j.isci.2022.104021.

Hashimoto, K., Joshi, S.K., and Koni, P.A. (2002). A conditional null allele of the major histocompatibility IA-beta chain gene. Genesis *32*, 152–153.

Hayashi, A., Sato, T., Kamada, N., Mikami, Y., Matsuoka, K., Hisamatsu, T., Hibi, T., Roers, A., Yagita, H., Ohteki, T., et al. (2013). A single strain of Clostridium butyricum induces intestinal IL-10-producing macrophages to suppress acute experimental colitis in mice. Cell Host Microbe *13*, 711–722. https://doi.org/10.1016/j.chom.2013.05.013.

Honda, K., and Littman, D.R. (2016). The microbiota in adaptive immune homeostasis and disease. Nature *535*, 75–84. https://doi.org/10.1038/nature18848.

Hori, S., Nomura, T., and Sakaguchi, S. (2003). Control of regulatory T cell development by the transcription factor Foxp3. Science *299*, 1057–1061. https://doi.org/10.1126/science.1079490.

Hsu, T.M., Welner, D.H., Russ, Z.N., Cervantes, B., Prathuri, R.L., Adams, P.D., and Dueber, J.E. (2018). Employing a biochemical protecting group for a sustainable indigo dyeing strategy. Nat. Chem. Biol. *14*, 256–261. https://doi.org/10.1038/nchembio.2552.

Jiang, X.L., and Cui, H.F. (2002). An analysis of 10218 ulcerative colitis cases in China. World J. Gastroenterol. *8*, 158–161. https://doi.org/10.3748/wjg.v8.i1.158.

Kamada, N., Seo, S.U., Chen, G.Y., and Núñez, G. (2013). Role of the gut microbiota in immunity and inflammatory disease. Nat. Rev. Immunol. *13*, 321–335. https://doi.org/10.1038/nri3430.

Kashiwagi, I., Morita, R., Schichita, T., Komai, K., Saeki, K., Matsumoto, M., Takeda, K., Nomura, M., Hayashi, A., Kanai, T., et al. (2015). Smad2 and Smad3 inversely regulate TGF-β autoinduction in Clostridium butyricum-activated dendritic cells. Immunity *43*, 65–79. https://doi.org/10.1016/j.immuni.2015.06.010.

Kataoka, H., Sugahara, K., Shimano, K., Teshima, K., Koyama, M., Fukunari, A., and Chiba, K. (2005). FTY720, sphingosine 1-phosphate receptor modulator, ameliorates experimental autoimmune encephalomyelitis by inhibition of T cell infiltration. Cell Mol. Immunol. *2*, 439–448.

Kawai, S., Iijima, H., Shinzaki, S., Hiyama, S., Yamaguchi, T., Araki, M., Iwatani, S., Shiraishi, E., Mukai, A., Inoue, T., et al. (2017). Indigo Naturalis ameliorates murine dextran sodium sulfate-induced colitis via aryl hydrocarbon receptor activation. J. Gastroenterol. *52*, 904–919. https://doi.org/10.1007/s00535-016-1292-z.

Kim, K.S., Hong, S.W., Han, D., Yi, J., Jung, J., Yang, B.G., Lee, J.Y., Lee, M., and Surh, C.D. (2016). Dietary antigens limit mucosal immunity by inducing regulatory T cells in the small intestine. Science *351*, 858–863. https://doi.org/10.1126/science.aac5560.

Koda, Y., Nakamoto, N., Chu, P.S., Ugamura, A., Mikami, Y., Teratani, T., Tsujikawa, H., Shiba, S., Taniki, N., Sujino, T., et al. (2019). Plasmacytoid dendritic cells protect against immune-mediated acute liver injury via IL-35. J. Clin. Invest. *129*, 3201–3213. https://doi.org/10.1172/jci125863.

Lamas, B., Richard, M.L., Leducq, V., Pham, H.P., Michel, M.L., Da Costa, G., Bridonneau, C., Jegou, S., Hoffmann, T.W., Natividad, J.M., et al. (2016). CARD9 impacts colitis by altering gut microbiota metabolism of tryptophan into aryl hydrocarbon receptor ligands. Nat. Med. *22*, 598–605. https://doi.org/10.1038/nm.4102.

Lehmann, J., Huehn, J., de la Rosa, M., Maszyna, F., Kretschmer, U., Krenn, V., Brunner, M., Scheffold, A., and Hamann, A. (2002). Expression of the integrin alpha Ebeta 7 identifies unique subsets of CD25+ as well as CD25- regulatory T cells. Proc. Natl. Acad. Sci. U.S.A. *99*, 13031–13036. https://doi.org/10.1073/pnas.192162899.

Li, W., Germain, R.N., and Gerner, M.Y. (2017). Multiplex, quantitative cellular analysis in large tissue volumes with clearing-enhanced 3D microscopy (C(e)3D). Proc. Natl. Acad. Sci. U.S.A. *114*, E7321-e7330. https://doi.org/10.1073/pnas.1708981114.

Littman, D.R., and Rudensky, A.Y. (2010). Th17 and regulatory T cells in mediating and restraining inflammation. Cell *140*, 845–858. https://doi.org/10.1016/j.cell.2010.02.021.

London, M., Bilate, A.M., Castro, T.B.R., Sujino, T., and Mucida, D. (2021). Stepwise chromatin and transcriptional acquisition of an intraepithelial lymphocyte program. Nat. Immunol. *22*, 449–459. https://doi.org/10.1038/s41590-021-00883-8.

Macosko, E.Z., Basu, A., Satija, R., Nemesh, J., Shekhar, K., Goldman, M., Tirosh, I., Bialas, A.R., Kamitaki, N., Martersteck, E.M., et al. (2015). Highly parallel genome-wide expression profiling of individual cells using nanoliter droplets. Cell *161*, 1202–1214. https://doi.org/10.1016/j.cell.2015.05.002.

Madisen, L., Zwingman, T.A., Sunkin, S.M., Oh, S.W., Zariwala, H.A., Gu, H., Ng, L.L., Palmiter, R.D., Hawrylycz, M.J., Jones, A.R., et al. (2010). A robust and high-throughput Cre reporting and characterization system for the whole mouse brain. Nat. Neurosci. *13*, 133–140. https://doi.org/10.1038/nn.2467.

McHugh, R.S., Whitters, M.J., Piccirillo, C.A., Young, D.A., Shevach, E.M., Collins, M., and Byrne, M.C. (2002). CD4(+)CD25(+) immunoregulatory T cells: gene expression analysis reveals a functional role for the glucocorticoid-induced TNF receptor. Immunity *16*, 311–323. https://doi.org/10.1016/s1074-7613(02)00280-7.

Mennigen, R., Nolte, K., Rijcken, E., Utech, M., Loeffler, B., Senninger, N., and Bruewer, M. (2009). Probiotic mixture VSL#3 protects the epithelial barrier by maintaining tight junction protein expression and preventing apoptosis in a murine model of colitis. Am. J. Physiol. Gastrointest. Liver Physiol. *296*, G1140–G1149. https://doi.org/10.1152/ajpgi.90534.2008.

Mezrich, J.D., Fechner, J.H., Zhang, X., Johnson, B.P., Burlingham, W.J., and Bradfield, C.A. (2010). An interaction between kynurenine and the aryl hydrocarbon receptor can generate regulatory T cells. J. Immunol. *185*, 3190–3198. https://doi.org/10.4049/jimmunol.0903670.

Miragaia, R.J., Gomes, T., Chomka, A., Jardine, L., Riedel, A., Hegazy, A.N., Whibley, N., Tucci, A., Chen, X., Lindeman, I., et al. (2019). Single-cell transcriptomics of regulatory T cells reveals trajectories of tissue adaptation. Immunity *50*, 493–504.e7. https://doi.org/10.1016/j.immuni.2019.01.001.

Miyara, M., Yoshioka, Y., Kitoh, A., Shima, T., Wing, K., Niwa, A., Parizot, C., Taflin, C., Heike, T., Valeyre, D., et al. (2009). Functional delineation and differentiation dynamics of human CD4+ T cells expressing the FoxP3 transcription factor. Immunity *30*, 899–911. https://doi.org/10.1016/j.immuni.2009.03.019.

Monteleone, I., Rizzo, A., Sarra, M., Sica, G., Sileri, P., Biancone, L., MacDonald, T.T., Pallone, F., and Monteleone, G. (2011). Aryl hydrocarbon receptor-induced signals up-regulate IL-22 production and inhibit inflammation in the gastrointestinal tract. Gastroenterology *141*, 237–248.e1. https://doi.org/10.1053/j.gastro.2011.04.007.

Morikawa, R., Nemoto, Y., Yonemoto, Y., Tanaka, S., Takei, Y., Oshima, S., Nagaishi, T., Tsuchiya, K., Nozaki, K., Mizutani, T., et al. (2021). Intraepithelial lymphocytes suppress intestinal tumor growth by cell-to-cell contact via CD103/E-cadherin signal. Cell Mol. Gastroenterol. Hepatol. *11*, 1483–1503. https://doi.org/10.1016/j.jcmgh.2021.01.014.

Mucida, D., Park, Y., Kim, G., Turovskaya, O., Scott, I., Kronenberg, M., and Cheroutre, H. (2007). Reciprocal TH17 and regulatory T cell differentiation mediated by retinoic acid. Science *317*, 256–260. https://doi.org/10.1126/science.1145697.

Naganuma, M., Sugimoto, S., Mitsuyama, K., Kobayashi, T., Yoshimura, N., Ohi, H., Tanaka, S., Andoh, A., Ohmiya, N., Saigusa, K., et al. (2018). Efficacy of indigo naturalis in a multicenter randomized controlled trial of patients with ulcerative colitis. Gastroenterology *154*, 935–947. https://doi.org/10.1053/j.gastro.2017.11.024.

Nishio, J., Baba, M., Atarashi, K., Tanoue, T., Negishi, H., Yanai, H., Habu, S., Hori, S., Honda, K., and Taniguchi, T. (2015). Requirement of full TCR repertoire for regulatory T cells to maintain intestinal homeostasis. Proc. Natl. Acad. Sci. U.S.A. *112*, 12770–12775. https://doi.org/10.1073/pnas.1516617112.

Nutsch, K., Chai, J.N., Ai, T.L., Russler-Germain, E., Feehley, T., Nagler, C.R., and Hsieh, C.S. (2016). Rapid and efficient generation of regulatory T cells to commensal antigens in the periphery. Cell Rep. *17*, 206–220. https://doi.org/10.1016/j.celrep.2016.08.092.

Ohkura, N., Kitagawa, Y., and Sakaguchi, S. (2013). Development and maintenance of regulatory T cells. Immunity *38*, 414–423. https://doi.org/10.1016/j.immuni.2013.03.002.

Pauls, K., Schön, M., Kubitza, R.C., Homey, B., Wiesenborn, A., Lehmann, P., Ruzicka, T., Parker, C.M., and Schön, M.P. (2001). Role of integrin alphaE(CD103)beta7 for tissue-specific epidermal localization of CD8+ T lymphocytes. J. Invest. Dermatol. *117*, 569–575. https://doi.org/10.1046/j.0022-202x.2001.01481.x.

Powrie, F., Leach, M.W., Mauze, S., Caddie, L.B., and Coffman, R.L. (1993). Phenotypically distinct subsets of CD4+ T cells induce or protect from chronic intestinal inflammation in C. B-17 scid mice. Int. Immunol. *5*, 1461–1471. https://doi.org/10.1093/intimm/5.11.1461.

Qiu, J., Heller, J.J., Guo, X., Chen, Z.M., Fish, K., Fu, Y.X., and Zhou, L. (2012). The aryl hydrocarbon receptor regulates gut immunity through modulation of innate lymphoid cells. Immunity *36*, 92–104. https://doi.org/10.1016/j.immuni.2011.11.011.

Quintana, F.J., Basso, A.S., Iglesias, A.H., Korn, T., Farez, M.F., Bettelli, E., Caccamo, M., Oukka, M., and Weiner, H.L. (2008). Control of T(reg) and T(H)17 cell differentiation by the aryl hydrocarbon receptor. Nature *453*, 65–71. https://doi.org/10.1038/nature06880.

Quintana, F.J., Murugaiyan, G., Farez, M.F., Mitsdoerffer, M., Tukpah, A.M., Burns, E.J., and Weiner, H.L. (2010). An endogenous aryl hydrocarbon receptor ligand acts on dendritic cells and T cells to suppress experimental autoimmune encephalomyelitis. Proc. Natl. Acad. Sci. U.S.A. *107*, 20768–20773. https://doi.org/10.1073/pnas.1009201107.

Raffin, C., Vo, L.T., and Bluestone, J.A. (2020). T(reg) cell-based therapies: challenges and perspectives. Nat. Rev. Immunol. *20*, 158–172. https://doi.org/10.1038/s41577-019-0232-6.

Rutgeerts, P., Sandborn, W.J., Feagan, B.G., Reinisch, W., Olson, A., Johanns, J., Travers, S., Rachmilewitz, D., Hanauer, S.B., Lichtenstein, G.R., et al. (2005). Infliximab for induction and maintenance therapy for ulcerative colitis. New Engl. J. Med. *353*, 2462–2476. https://doi.org/10.1056/nejmoa050516.

Sakaguchi, S., Miyara, M., Costantino, C.M., and Hafler, D.A. (2010). FOXP3+ regulatory T cells in the human immune system. Nat. Rev. Immunol. *10*, 490–500. https://doi.org/10.1038/nri2785.

Sakaguchi, S., Vignali, D.A., Rudensky, A.Y., Niec, R.E., and Waldmann, H. (2013). The plasticity and stability of regulatory T cells. Nat. Rev. Immunol. *13*, 461–467. https://doi.org/10.1038/nri3464.

Sakaguchi, S., Yamaguchi, T., Nomura, T., and Ono, M. (2008). Regulatory T cells and immune tolerance. Cell *133*, 775–787. https://doi.org/10.1016/j.cell.2008.05.009.

Schiering, C., Krausgruber, T., Chomka, A., Fröhlich, A., Adelmann, K., Wohlfert, E.A., Pott, J., Griseri, T., Bollrath, J., Hegazy, A.N., et al. (2014). The alarmin IL-33 promotes regulatory T-cell function in the intestine. Nature *513*, 564–568. https://doi.org/10.1038/nature13577.

Schiering, C., Wincent, E., Metidji, A., Iseppon, A., Li, Y., Potocnik, A.J., Omenetti, S., Henderson, C.J., Wolf, C.R., Nebert, D.W., et al. (2017). Feedback control of AHR signalling regulates intestinal immunity. Nature *542*, 242–245. https://doi.org/10.1038/nature21080.

Schön, M.P., Arya, A., Murphy, E.A., Adams, C.M., Strauch, U.G., Agace, W.W., Marsal, J., Donohue, J.P., Her, H., Beier, D.R., et al. (1999). Mucosal T lymphocyte numbers are selectively reduced in integrin alpha E (CD103)-deficient mice. J. Immunol. *162*, 6641–6649.

Sefik, E., Geva-Zatorsky, N., Oh, S., Konnikova, L., Zemmour, D., McGuire, A.M., Burzyn, D., Ortiz-Lopez, A., Lobera, M., Yang, J., et al. (2015). Mucosal immunology. Individual intestinal symbionts induce a distinct population of RORγ$^+$ regulatory T cells. Science *349*, 993–997. https://doi.org/10.1126/science.aaa9420.

Shevach, E.M. (2009). Mechanisms of foxp3+ T regulatory cell-mediated suppression. Immunity *30*, 636–645. https://doi.org/10.1016/j.immuni.2009.04.010.

Sontheimer-Phelps, A., Chou, D.B., Tovaglieri, A., Ferrante, T.C., Duckworth, T., Fadel, C., Frismantas, V., Sutherland, A.D., Jalili-Firoozinezhad, S., Kasendra, M., et al. (2020). Human colon-on-a-chip enables continuous in vitro analysis of colon mucus layer accumulation and physiology. Cell Mol. Gastroenterol. Hepatol. *9*, 507–526. https://doi.org/10.1016/j.jcmgh.2019.11.008.

Stephens, W.Z., Kubinak, J.L., Ghazaryan, A., Bauer, K.M., Bell, R., Buhrke, K., Chiaro, T.R., Weis, A.M., Tang, W.W., Monts, J.K., et al. (2021). Epithelial-myeloid exchange of MHC class II constrains immunity and microbiota composition. Cell Rep. *37*, 109916. https://doi.org/10.1016/j.celrep.2021.109916.

Stockinger, B., Di Meglio, P., Gialitakis, M., and Duarte, J.H. (2014). The aryl hydrocarbon receptor: multitasking in the immune system. Annu. Rev. Immunol. *32*, 403–432. https://doi.org/10.1146/annurev-immunol-032713-120245.

Suffia, I., Reckling, S.K., Salay, G., and Belkaid, Y. (2005). A role for CD103 in the retention of CD4+CD25+ Treg and control of Leishmania major infection. J. Immunol. *174*, 5444–5455. https://doi.org/10.4049/jimmunol.174.9.5444.

Sugimoto, S., Naganuma, M., and Kanai, T. (2016a). Indole compounds may be promising medicines for ulcerative colitis. J. Gastroenterol. *51*, 853–861. https://doi.org/10.1007/s00535-016-1220-2.

Sugimoto, S., Naganuma, M., Kiyohara, H., Arai, M., Ono, K., Mori, K., Saigusa, K., Nanki, K., Takeshita, K., Takeshita, T., et al. (2016b). Clinical efficacy and safety of oral Qing-Dai in patients with ulcerative colitis: a single-center open-label prospective study. Digestion *93*, 193–201. https://doi.org/10.1159/000444217.

Sugita, K., Hanakawa, S., Honda, T., Kondoh, G., Miyachi, Y., Kabashima, K., and Nomura, T. (2015). Generation of Helios reporter mice and an evaluation of the suppressive capacity of Helios(+) regulatory T cells in vitro. Exp. Dermatol. *24*, 554–556. https://doi.org/10.1111/exd.12711.

Sugiyama, D., Nishikawa, H., Maeda, Y., Nishioka, M., Tanemura, A., Katayama, I., Ezoe, S., Kanakura, Y., Sato, E., Fukumori, Y., et al. (2013). Anti-CCR4 mAb selectively depletes effector-type FoxP3+CD4+ regulatory T cells, evoking antitumor immune responses in humans. Proc. Natl. Acad. Sci. U.S.A. *110*, 17945–17950. https://doi.org/10.1073/pnas.1316796110.

Sujino, T., Kanai, T., Ono, Y., Mikami, Y., Hayashi, A., Doi, T., Matsuoka, K., Hisamatsu, T., Takaishi, H., Ogata, H., et al. (2011). Regulatory T cells suppress development of colitis, blocking differentiation of T-helper 17 into alternative T-helper 1 cells. Gastroenterology *141*, 1014–1023. https://doi.org/10.1053/j.gastro.2011.05.052.

Sujino, T., London, M., Hoytema van Konijnenburg, D.P., Rendon, T., Buch, T., Silva, H.M., Lafaille, J.J., Reis, B.S., and Mucida, D. (2016). Tissue adaptation of regulatory and intraepithelial CD4$^+$ T cells controls gut inflammation. Science (New York, NY) *352*, 1581–1586.

Tanoue, T., Atarashi, K., and Honda, K. (2016). Development and maintenance of intestinal regulatory T cells. Nat. Rev. Immunol. *16*, 295–309. https://doi.org/10.1038/nri.2016.36.

Thornton, A.M., Korty, P.E., Tran, D.Q., Wohlfert, E.A., Murray, P.E., Belkaid, Y., and Shevach, E.M. (2010). Expression of Helios, an Ikaros transcription factor family member, differentiates thymic-derived from peripherally induced Foxp3+ T regulatory cells. J. Immunol. *184*, 3433–3441. https://doi.org/10.4049/jimmunol.0904028.

Turner, D., Walsh, C.M., Steinhart, A.H., and Griffiths, A.M. (2007). Response to corticosteroids in severe ulcerative colitis: a systematic review of the literature and a meta-regression. Clin. Gastroenterol. Hepatol. *5*, 103–110. https://doi.org/10.1016/j.cgh.2006.09.033.

Voskoboinik, I., Whisstock, J.C., and Trapani, J.A. (2015). Perforin and granzymes: function, dysfunction and human pathology. Nat. Rev. Immunol. *15*, 388–400. https://doi.org/10.1038/nri3839.

Whibley, N., Tucci, A., and Powrie, F. (2019). Regulatory T cell adaptation in the intestine and skin. Nat. Immunol. *20*, 386–396. https://doi.org/10.1038/s41590-019-0351-z.

Wohlfert, E.A., Grainger, J.R., Bouladoux, N., Konkel, J.E., Oldenhove, G., Ribeiro, C.H., Hall, J.A., Yagi, R., Naik, S., Bhairavabhotla, R., et al. (2011). GATA3 controls Foxp3$^+$ regulatory T cell fate during inflammation in mice. J. Clin. Invest. *121*, 4503–4515. https://doi.org/10.1172/jci57456.

Xiao, H.T., Peng, J., Hu, D.D., Lin, C.Y., Du, B., Tsang, S.W., Lin, Z.S., Zhang, X.J., Lueng, F.P., Han, Q.B., et al. (2015). Qing-Dai powder promotes recovery of colitis by inhibiting inflammatory responses of colonic macrophages in dextran sulfate sodium-treated mice. Chin. Med. *10*, 29. https://doi.org/10.1186/s13020-015-0061-x.

Xu, M., Pokrovskii, M., Ding, Y., Yi, R., Au, C., Harrison, O.J., Galan, C., Belkaid, Y., Bonneau, R., and Littman, D.R. (2018). c-MAF-dependent regulatory T cells mediate immunological tolerance to a gut pathobiont. Nature *554*, 373–377. https://doi.org/10.1038/nature25500.

Ye, J., Qiu, J., Bostick, J.W., Ueda, A., Schjerven, H., Li, S., Jobin, C., Chen, Z.E., and Zhou, L. (2017). The aryl hydrocarbon receptor preferentially marks and promotes gut regulatory T cells. Cell Rep. *21*, 2277–2290. https://doi.org/10.1016/j.celrep.2017.10.114.

Yoshimatsu, Y., Naganuma, M., Sugimoto, S., Tanemoto, S., Umeda, S., Fukuda, T., Nomura, E., Yoshida, K., Ono, K., Mutaguchi, M., et al. (2020). Development of an indigo naturalis suppository for topical induction therapy in patients with ulcerative colitis. Digestion *101*, 492–498. https://doi.org/10.1159/000501152.

Yoshimura, A., and Muto, G. (2011). TGF-β function in immune suppression. Curr. Top. Microbiol. Immunol. *350*, 127–147. https://doi.org/10.1007/82_2010_87.

Yu, F., Sharma, S., Edwards, J., Feigenbaum, L., and Zhu, J. (2015). Dynamic expression of transcription factors T-bet and GATA-3 by regulatory T cells maintains immunotolerance. Nat. Immunol. *16*, 197–206. https://doi.org/10.1038/ni.3053.

Zegarra-Ruiz, D.F., Kim, D.V., Norwood, K., Kim, M., Wu, W.H., Saldana-Morales, F.B., Hill, A.A., Majumdar, S., Orozco, S., Bell, R., et al. (2021). Thymic development of gut-microbiota-specific T cells. Nature *594*, 413–417. https://doi.org/10.1038/s41586-021-03531-1.

STAR★METHODS

KEY RESOURCES TABLE

REAGENT or RESOURCE	SOURCE	IDENTIFIER
Antibodies		
CD4 (clone: RM4-5; BV421)	Biolegend	Cat# 100544; RRID: AB_11219790
CD8α (clone: 53-6.7; PE-Cy7)	BD Bioscience	Cat# 552877; RRID: AB_394506
CD8β (clone: eBioH35-17.2; APC)	eBioscience	Cat# 17-0083-81; RRID: AB_657760
CD25 (clone: PC61.5; PE)	eBioscience	Cat#; 12-0251-83; RRID: AB_465607
CD44 (clone: IM7; APC)	Biolegend	Cat# 103012; RRID: AB_312963
CD45 (clone: 30-F11; BV510)	Biolegend	Cat# 103138; RRID: AB_2563061
CD45RB (clone: C363.16A; PE)	eBioscience	Cat#; 12-0455-82 RRID: AB_465681
CD45.1 (clone: A20; PerCP-Cy5.5)	eBioscience	Cat#45-0453-82; RRID: AB_1107003
CD45.2 (clone: 104; PE-Cy7)	Biolegend	Cat#109830; RRID: AB_1186098
CD62L (clone: MEL-14; FITC)	Biolegend	Cat# 104406; RRID: AB_313093
CD103 (clone: 2-E7; FITC)	Biolegend	Cat#121419; RRID: AB_10714791
CD326 (Ep-CAM) (clone: G8.8; APC)	Biolegend	Cat#118212; RRID: AB_1134102
CTLA-4 (clone: UC10-4F10-11; PE)	BD Bioscience	Cat#553720; RRID: AB_395005
TCRβ (clone: H57-597; APC-Cy7)	Biolegend	Cat# 109220; RRID: AB_893624
TCRγδ (clone: GL3; PerCP-Cy5.5)	Biolegend	Cat# 118117; RRID: AB_10612572
Foxp3 (clone: FJK-16s; PE)	eBioscience	Cat# 12-5773-82; RRID: AB_465936
Gata-3 (clone: TWAJ; FITC)	eBioscience	Cat#53-9966-42; RRID: AB_1963600
Rorγt (clone: Q31-378; BV421)	BD Bioscience	Cat# 562894; RRID: AB_2687545
Helios (clone: 22F6; PE)	Biolegend	Cat#137216; RRID: AB_10660749
Granzyme A (clone:GzA-3G8.5; APC)	eBioscience	Cat#17-5831-80; RRID: AB_2573228
c-MAF (clone:sym0F1; eFluor 660)	eBioscience	Cat#50-9855-80; RRID: AB_2574388
T-bet (clone: 4B10; APC)	Biolegend	Cat#644814; RRID: AB_10901173
IL-17A (clone: eBio17B7; PE)	eBioscience	Cat# 12-7177-81; RRID: AB_763582
IFNγ (clone: XMG1.2; FITC)	eBioscience	Cat# 11-7311-82; RRID: AB_465412
IL-22 (clone: IL-22JOP; APC)	eBioscience	Cat# 11-7311-82; RRID: AB_465412
E-Cadherin (clone: 36/E-Cadherin; FITC)	BD Bioscience	Cat#612131; RRID: AB_2076677
I-A/I-E (clone: M5/114.15.2; PerCP-Cy5.5)	Biolegend	Cat#107626; RRID: AB_2191071
IL-33Rα (ST2) (clone: DIH9; BV421)	Biolegend	Cat#145309; RRID: AB_2565634
CD3e (clone: 145-2C11)	Biolegend	Cat# 100359; RRID: AB_2616673
Chemicals, peptides, and recombinant proteins		
Tamoxifen	Sigma-Aldrich	Cat# T5648
Corn oil	Wako	Cat# 032-17016
Phorbol 12-myristate 13-acetate (PMA)	Sigma-Aldrich	Cat# P8139
Ionomycin	Sigma-Aldrich	Cat# I9657
FTY720≧98%(HPLC)	Sigma-Aldrich	Cat# SML0700
L-Buthionine-sulfoximine≧97%(TLC)	Sigma-Aldrich	Cat# B2515-1G
Zinc Protoporphyrin-9	CAYMAN	Cat# 14483
Fixable Viability Dye eFluor 780	eBioscience	Cat# 65-0865-14
Click-iT™ Plus EdU Alexa Fluor™ 647 Flow Cytometry Assay Kit	Thermo Fisher Scientific	Cat# C10635
Mouse Lipocalin-2/NGAL Duoset Kit ELISA, 5-Plate	R&D Systems	Cat# DY1857-05
Dithiothreitol (DTT)	Thermo Fisher Scientific	Cat# P2325
EDTA	Nacalai Tesque	Cat# 06894-85
Collagenase	Wako	Cat# 032-22364

(*Continued on next page*)

Continued

REAGENT or RESOURCE	SOURCE	IDENTIFIER
DNase I	Sigma-Aldrich	Cat# DN25
Percoll	GE Healthcare	Cat# 1789101
Ammonium chloride	Nacalai Tesque	Cat# 02424-55
4% Paraformaldehyde Phosphate Buffer Solution	Wako	Cat# 163-20145
8% Glutaraldehyde	Wako	Cat# 533-08681
Agarose LM	Nacalai Tesque	Cat# 01161-54
Bovine serum albumin (BSA)	Nacalai Tesque	Cat# 01863-48
Triton-X100	Polysciences	Cat# 04605
DAPI	Dojindo	Cat# D523
Mouse Naïve $CD4^+$ T cell isolation kit	Miltenyi Biotech	Cat# 130-104-453
TGF-β	R&D systems	Cat# 7666-MB-005
Retinoic acid (RA)	Tokyo Chemical Industry	Cat# 0064-1G
IFN-γ	Peprotech	Cat# 315-05
Fetal bovine serum (FBS)	Thermo Fisher Scientific	Cat# 10270-106
HBSS	Nacalai Tesque	Cat# 17460-15
RPMI1640	Nacalai Tesque	Cat# 30264-85
DPBS	Nacalai Tesque	Cat# 14249-24
Penicillin/streptmycin	Nacalai Tesque	Cat# 09367-34
Sodium pyruvate	Thermo Fisher Scientific	Cat# 11360070
MEM/NEAA	Thermo Fisher Scientific	Cat# 11140050
HEPES	Thermo Fisher Scientific	Cat# 15630080
1 mg/mL Mitomycin C Solution	FUJIFILM	Cat# 133-15931
β-mercaptoethanol	Thermo Fisher Scientific	Cat# 21985023
TRIzol	Invitrogen	Cat# 15596018
Critical commercial assays		
iScript cDNA Synthesis Kit	BioRad	Cat# 170-8891
SYBR Green FAST qPCR Master Mix kit	Kapa Biosystems	Cat# KK4602
Foxp3/transcription factor staining buffer set	eBioscience	Cat# 00-5523-00
GoldiStop Protein Transport Inhibitor	BD Bioscience	Cat# 554724; RRID: AB_2869012
Experimental models: Organisms/strains		
Mouse: C57BL/6J	The Jackson Laboratory	JAX:000664
Mouse: *Cd4*^{creERT2}	The Jackson Laboratory	JAX:022356
Mouse: *Villin*^{creERT2}	The Jackson Laboratory	JAX:020282
Mouse: *Foxp3*$^{eGFP\text{-}cre\text{-}ERT2}$	The Jackson Laboratory	JAX:016961
Mouse: *H2ab1*$^{fl/fl}$	(Hashimoto et al., 2002)	N.A.(Gruber et al., 2007)
Mouse: *Ahr*$^{fl/fl}$	The Jackson Laboratory	JAX:006203
Mouse: *Helios*^{venus}	(Sugita et al., 2015)	N.A.
Mouse: *Rosa26*$^{lsl\text{-}tdtomato}$	(Madisen et al., 2010)	N.A.
Oligonucleotides		
QPCR primers	Hokkaido System Science	Table S1
Software and algorithms		
GraphPad Prism 8	GraphPad Software	https://www.graphpad.com/
FlowJo Vx software	TreeStar	https://www.flowjo.com/
ImageJ	ImageJ	https://imagej.net/Welcome
Imaris 8.4	Bitplane	https://imaris.oxinst.com
Deposited data		
Raw RNA sequencing of Treg	the DDBJ BioProject	https://ddbj.nig.ac.jp/resource/bioproject/PRJDB13371 (DRA013836)

(*Continued on next page*)

Continued

REAGENT or RESOURCE	SOURCE	IDENTIFIER
Raw RNA sequencing of IEC	the DDBJ BioProject	https://ddbj.nig.ac.jp/resource/bioproject/PRJDB13371 (DRA013837)
Raw RNA single cell sequencing of Treg	the DDBJ BioProject	https://ddbj.nig.ac.jp/resource/bioproject/PRJDB13371 (DRA013838)
Raw 16S rRNA sequence	the DDBJ BioProject	https://ddbj.nig.ac.jp/resource/bioproject/PRJDB13371 (DRA013839)

RESOURCE AVAILABILITY

Lead contact

Further information and requests for the resources and reagents should be directed and will be fulfilled by the Lead Contact, Tomohisa Sujino (tsujino1224@keio.jp).

Materials availability

All the mouse lines used in this study are available upon request.

This study did not generate new reagents.

Data and code availability

Raw data from RNA-seq experiments have been deposited at RDA and are publicly available as of the date of publication. Accession numbers are listed in the key resources table.

This paper does not report original code.

All data reported in this paper will be shared by the lead contact upon request.

Any additional information required to reanalyze the data reported in this paper is available from the lead contact upon request.

EXPERIMENTAL MODEL AND SUBJECT DETAILS

Patients

Colon tissue samples were obtained from patients with UC treated with existing therapies (n = 3) or IN (n = 3). Human colon epithelium was isolated from colon re-sections or endoscopic tissue biopsy specimens. UC was diagnosed by the criteria defined by the research group of inflammatory bowel disease at the Ministry of Health, Labour and Welfare in Japan. All experiments were approved by the institutional review board of Keio University School of Medicine, and written informed consent was obtained from all patients, in accordance with the Declaration of Helsinki. We used in total 6 of individual donors of human colon tissue samples within age range 27–56, median age (IQR) 47.5 (42.5–50.25). Age of patients is not significantly different between two groups.

Animals

Adult male C57BL6/J mice (6–7 weeks) were purchased from CLEA Japan (Tokyo, Japan). GF (C57BL6/N background) mice were purchased from Sankyo Labo Service Corporation (Tokyo, Japan). *Foxp3*$^{eGFP\text{-}CreER}$ mice, *Ahr* $^{fl/fl}$ mice, *Vilin* $^{Cre\text{-}ER}$ mice, and *Cd4*$^{Cre\text{-}ER}$ mice were purchased from Jackson Laboratories. *Rosa26*$^{lsl\text{-}tdTomato}$ mice were kindly provided by Dr. Hongkui Zeng (Allen Institute, USA). *Helios*^{Venus} mice were kindly provided by Kenji Kabashima. Takashi Nomura (Department of Dermatology, Kyoto U.). *H2Ab* $^{fl/fl}$ mice were kindly provided by Yasuo Nemoto (Tokyo Medical and Dental U.). Mice, except for GF mice, were maintained under specific pathogen-free (SPF) conditions. GF mice were bred and maintained in vinyl isolators. Genotyping was performed according to the protocols established for the respective strains by Jackson Laboratories. All experiments were approved by the Institutional Review Board for Animal Experiments at Keio University and were performed according to the institutional guidelines and home office regulations.

METHOD DETAILS

Tamoxifen treatment

Helios^{Venus};*Rosa26*$^{lsl\_tdTomato}$; *Foxp3*$^{eGFP\text{-}CreER}$ mice were gavaged for two consecutive days with 200 mg/kg of tamoxifen (Sigma, USA) 24 hours prior to sacrifice or intravital imaging. *Vilin*$^{Cre\text{-}ER}$;*Ahr*$^{fl/fl}$ mice, *Vilin*$^{Cre\text{-}ER}$;*H2Ab1*$^{fl/fl}$ and *Cd4*$^{Cre\text{-}ER}$;*Ahr*$^{fl/fl}$ mice were intraperitoneally (I.P.) injected for 4 days (two consecutive days within one week) with 100 mg/kg of tamoxifen. Tamoxifen was dissolved in corn oil (Wako) at 10 mg/mL.

Induction of colitis by DSS

Colitis was induced by the addition of 2% (wt/vol) dextran sodium sulphate (DSS; molecular weight: 36,000–50,000; MP Biomedicals, Solon, OH, USA) to the sterile drinking water given to the mice. On days 6–7 after DSS administration, the supplementation was discontinued and untreated water was provided for 1–2 days, and the mice were sacrificed. Clinical assessment of all DSS-treated animals for body weight and general appearance was performed daily. SPF mice were weighed every day to determine the percentage of body weight loss from baseline. Body weight loss, stool consistency, and rectal bleeding were evaluated and scored for the disease activity index (DAI) (Hayashi et al., 2013). No weight loss was registered as 0, weight loss of 1% to 5% from baseline was assigned 1 point, weight loss of 6% to 10% from baseline was assigned 2 points, weight loss of 11% to 20% from baseline was assigned 3 points, and weight loss of more than 20% from baseline was assigned 4 points. For stool consistency, 0 points were assigned for well-formed pellets, 2 points for paste-like and semi-formed stools that did not adhere to the anus, and 4 points for liquid stools that adhered to the anus. For bleeding, a score of 0 was assigned for no blood, 2 for positive bleeding, and 4 for gross bleeding. The colons were excised and their lengths documented. The degree of inflammation and epithelial damage was determined by microscopic examination of haematoxylin and eosin (H&E)-stained sections of the colon as described below.

Adoptive transfer

$CD4^+$ T cells were isolated from the spleens of C57BL/6J ($Ly5.1^+$) mice using the anti-CD4 (L3T4) MACS magnetic separation system (Miltenyi Biotec). Enriched $CD4^+$ T cells were stained with CD4, CD45RB and CD25 mAbs, then sorted to yield the $CD4^+CD25^-CD45RB^{high}$ fraction using FACSAria (Becton Dickinson, NJ, USA). $Tomato^+$ $CD4^+$ T cells of spleen, mesenteric lymph node (mLN) and colon lamina propria were obtained from *Rosa26*$^{lsl\text{-}tdTomato}$ x *Foxp3*$^{eGFP\text{-}Cre\text{-}ERT2}$ mice. Purified $CD4^+CD45RB^{high}$ (3.0×10^5 cells/mouse) alone or in combination with $Tomato^+$ $CD4^+$ T cells (3.75×10^4 cells/mouse) were intraperitoneally injected into RAG-$2^{-/-}$ mice. Mice were sacrificed at the indicated time point after transfer. Mice were assessed for a clinical score as the sum of 4 parameters: hunching and wasting, 0 or 1; colon thickening, 0–3 (0, no colon thickening; 1, mild thickening; 2, moderate thickening; 3, extensive thickening); and stool consistency, 0–3 (0, normal beaded stool; 1, soft stool; 2, diarrhoea), and an additional point was added if gross blood was noted (Sujino et al., 2011).

Antibiotic treatment

Antibiotics (ampicillin (6.7 g/L; SigmaAldrich), metronidazole (6.7 g/L; Sigma Aldrich), vancomycin (3.3 g/L; Sigma Aldrich), or neomycin sulfate (6.7 g/L; Sigma Aldrich) were dissolved in sterile distilled water in the final concentrations, and were administered to mice (500 μL per mouse) by oral gavage 3 times a week.

In vitro Treg suppression assay

Naive $CD4^+$ cells and $CD11c^+$ antigen presenting cells (APC) were isolated from spleen in C57BL/6J ($Ly5.1^+$) mice using naïve $CD4^+CD62L^+$ T cell and $CD11c^+$ isolation kit, respectively. $Tomato^+$ $CD4^+$ T cells of colon lamina propria were obtained from *Rosa26*$^{lsl\text{-}tdTomato}$ x *Foxp3*$^{eGFP\text{-}Cre\text{-}ERT2}$ mice with Ctrl-diet or IN diet using FACS Aria. To evaluate the effect of Tregs on T cell proliferation, naive $CD4^+$ cells were stained by a diluted solution of violet proliferation dye (VPD450; BD Biosciences) at 37°C for 15 minutes and $CD11c^+$ APCs were treated with 50 μg/mL of Mitomycin C (Wako, Tokyo, Japan) at 37°C for 30 minutes as previously described (Campos-Mora et al., 2019; Koda et al., 2019). Naive $CD4^+$ cells (4×10^4) alone or in combination with $Tomato^+$ $CD4^+$ T cells (2×10^4) were cultured in RPMI-1640 medium supplemented with 10% fetal bovine serum, 100 U/mL penicillin, 100 μg/mL streptomycin,25 mM HEPES, 1 mM sodium pyruvate, 1x MEM/NEAA and 55 μM 2-mercaptoethanol in a 96-well plate. Naive T cells were stimulated in the presence of soluble α-CD3 (2 μg/mL) for 3 days with $CD11c^+$APCs from spleen (5×10^4). used as (APC) After incubation, the cells were washed and cell proliferation was assessed by flow cytmetry.

Histology

A distal colon section after DSS-induced colitis and a skin section after induction of psoriasis-like dermatitis were collected and fixed with 10% formalin (068-03841, lot TWE1483; Wako, Tokyo, Japan). The fixed samples were embedded in paraffin and stained with H&E by Morphotechnology Co, Ltd (Sapporo, Japan). To evaluate the severity of DSS-induced colitis, the histological activity score (Mennigen et al., 2009) (maximum total score 40) was assessed as the sum of three parameters (extent, inflammation, and crypt damage) as follows: extent was scored as 0 to 3 (0, none; 1, mucosa; 2, submucosa; 3, transmural); inflammation was scored as 0 to 3 (0, none; 1, slight; 2, moderate; 3, severe); and crypt damage was scored as 0 to 4 (0, none; 1, basal one-third lost; 2, basal two-thirds lost; 3, only surface epithelium intact; 4, entire crypt and epithelium lost). There scores were multiplied by the scores for spread, which were from 1 to 4 (1, 0%–25%; 2, 26%–50%; 3, 51%–75%; 4, 76%–100%). Each multiplied score was summed and defined as a histologic score (0–40). To evaluate the severity of the adoptive transfer colitis, the most affected area of the pathological specimens was assessed for a histological score as the sum of three criteria: cell infiltration, crypt elongation, and number of crypt abscesses. Each was scored on a scale of 0–3 in a blinded fashion.

Immunohistochemistry

Human colon samples were fixed in 2% PFA at 4°C on a rocker overnight. All samples were blocked and permeabilized using 0.1% Triton X-100 (04605, Polysciences, Inc., Warrington, PA) and 5% bovine serum albumin (BSA) (01863-48; Nacalai Tesque) in DPBS

for 1 hour at room temperature (Sontheimer-Phelps et al., 2020). Samples then were stained overnight at 4°C in 2% BSA in DPBS with the following conjugated antibodies: anti-human CD25 (BC96, 1:200; eBioscience) and Phalloidin-iFluor™ 647 Conjugate (20555, 1:2000; Cayman Chemical, Ann Arbor, MI). Murine colon tissues were fixed in 4% PFA at 4°C on a rocker overnight. Fixed tissues were washed 3 times for 20 min in DPBS, embedded in 4% low melting point agarose (Nacarai Tesque), and cut into 200 μm sections with a vibratome (VT1200S; Leica, Wetzlar, Germany). Sections were incubated for at least 8 hours in a blocking buffer (DPBS containing 1% normal mouse serum, 1% bovine serum albumin and 0.3% Triton X-100). Tissues were then incubated with the following conjugated antibodies diluted 1:100 in blocking buffer: anti-mouse Ep-CAM Alexa Fluor 488 (G8.8; Bio Legend, San Diego, CA, USA), anti-mouse I-A/I-E Alexa Fluor 488 (M5/114.15.2; Bio Legend) and anti-mouse CD4 Brilliant Violet 421 (RM4-5; Bio Legend), for overnight at room temperature on a shaker. Images were taken using a laser scanning confocal microscope (Olympus FV3000; Olympus, Tokyo, Japan). Acquired images were analysed using IMARIS (Bitplane, Zurich, Switzerland) software.

Ce3D clearing and imaging of whole mount tissue

For volumetric imaging of mouse colon, the whole mount specimens were subjected to tissue clearing using Ce3D protocol as previously reported (Li et al., 2017). Fixed and stained whole mount specimens were washed in washing buffer (DPBS containing 0.2% Triton X-100 and 0.5% (v/v) 1-thioglycerol) for 1 day at room temperature. Washed samples were then dried on a Kimwipe and immediately immersed in Ce3D clearing solution (DPBS containing 22% (v/v) N-methylacetamide, 0.8 g/mL Histodenz, 0.1% (v/v) Triton X-100 and 0.5% (v/v) 1-thioglycerol) for 1 day at room temperature. Cleared tissues were embedded in a glass-bottom 35 mm dish with fresh Ce3D clearing solution and tightly sealed with a cover slip. Tissues were scanned in every 5 μm of z-axis by multiphoton confocal microscope (A1R-MP; Nikon, Tokyo, Japan) equipped with a Ti: sapphire laser (MaiTai eHP DeepSee, SpectoraPhysics, Santa Clara, CA). Acquired images were analysed using IMARIS (Bitplane) software.

Multi-photon intravital imaging and cell tracking

For Treg imaging, *Foxp3*$^{eGFP\text{-}CreER}$ mice were crossed with *Rosa26*$^{lsl\text{-}tdTomato}$ mice to obtain *Foxp3*$^{eGFP\text{-}CreER}$: *Rosa26*$^{lsl\text{-}tdTomato}$ mice (*iFoxp3*^{Tomato}). Mice were gavaged for two consecutive days with 200 mg/kg of tamoxifen prior to intravital imaging. Animals were anesthetized with 15 mL per gram of tribromorthanol (Avertin) and kept on 1% isoflurane oxygen mixture throughout the procedure. A 1 cm incision was made in the abdominal skin along the midline and colon was carefully externalized with tweezers. Then 1 cm incision was made along the colon and two additional perpendicular incisions were made to expose the luminal surface. Intravital imaging was performed using multiphoton confocal microscope (A1R-MP; Nikon) equipped with a Ti: sapphire laser (MaiTai eHP DeepSee, SpectoraPhysics). 30 μm z-stack images were acquired for 10 minutes with minimum intervals. IMARIS (Bitplane) software was used to generate volume-rendered 4D movies and for semiautomated tracking of cell motility.

ELISA for lipocalin-2

Lipocalin-2 was analysed by using the Lcn-2 ELISA kit (R&D, MN) as previously described (Chassaing et al., 2012).

FTY720 treatment

FTY720 (1 mg/kg) dissolved in distilled water or distilled water was administered orally to mice once a day from the start date of the special feedings according to the methods described previously (Kataoka et al., 2005).

Isolation of colon IELs and LPLs

The isolation of intraepithelial lymphocytes (IELs) and intestinal lamina propria lymphocytes (LPL) was conducted as previously described (Mucida et al., 2007). In brief, the large and small intestines were dissected, and fat tissue and Payer's patches were removed. The intestines were cut open longitudinally and washed in HBSS, then cut into 1-cm pieces, washed, and shaken in HBSS containing 1 mM DTT (Sigma-Aldrich, St. Louis, MO) and 0.5 M EDTA (Thermo Fisher Scientific, Waltham, MA) for 30 min at 37°C. The supernatant of the solution was harvested for epithelial cells by passing through a 100-μm cell strainer into a 50-mL Falcon tube. The cells were pelleted through 40% isotonic Percoll solution, then subjected to Ficoll-Hypaque density gradient centrifugation (40/75%). At the same time, the tissues without the epithelial cells were digested in HBSS medium containing bovine deoxyribonuclease I (Sigma) and collagenase (FUJIFILM Wako Pure Chemical Corporation, Japan) at 37°C for 30 min and 40 min for the small intestine and colon, respectively. The digested tissues were also homogenized by vigorous shaking and passed through a 100-μm cell strainer into a 50-mL Falcon tube with 1% EDTA, followed by a gradient centrifuge step with Percoll, as described for the epithelial cells. Both IELs and lamina propria mononuclear cells were collected at the interphase of the Percoll gradient, washed, and resuspended in FACS buffer or RPMI-1640 (Sigma) containing 10% FBS and penicillin/streptomycin (Gibco, Carlsbad, CA, USA).

Flow cytometric analysis

Fluorescent-dye-conjugated antibodies were purchased from BD Pharmingen (USA) (anti-E-Cadherin, 36/E-Cadherin; anti-RORgt, Q31-378; anti-ICOS, 7E.17G9; anti-GITR, DTA-1; anti-CD45.2, 104), eBioscience (anti-CD45.1, A20; anti-Foxp3, FJK-16s; anti-GATA3, TWAJ; anti-IL-7Ra, A7R34; anti-CXCR3, CXCR3-173; anti-CCR7, 4B12; anti-CD45RB, C363.16A; anti-CD25, PC61.5; anti-CD8a, 53-6.7; anti-IL-17A, eBio17B7; anti-IFN-g, XMG1.2; anti-IL-22, IL-22JOP) and Bio Legend (anti-CD326, Ep-CAM; G8.8; anti-CD45, 30-F11; anti-CD103, 2-E7; anti-ST2, DIH9; anti-CD3e, 145-2C11; anti-CD44, IM7; anti-CD62L, MEL-14; anti-CCR6,

29-2L17; anti-Helios, 22F6; anti-T-bet, 4B10; anti-CD4, RM4-5; anti-TCRb, H57-597; anti-I-A/I-E, M5/114.15.2). FACS data were acquired on a FACSCanto II (Becton, Dickinson, NJ, USA) and analysed by FlowJo (Tree Star, Inc. Ashland, OR, USA). Intracellular staining was conducted using the Foxp3 Mouse Regulatory T Cell Staining Kit (eBioscience, USA). For flow cytometric analysis of cytokine-secreting cells, the cells were resuspended in RPMI 1640 after isolation of lymphocytes from the colon. To stimulate cells, they were incubated at 37°C under 5% CO_2 in the presence of 50 ng/mL PMA (Sigma), 1 μg/mL Ionomycin (Sigma) and 50 ng/mL mouse IL-23 recombinant protein (eBioscience) (for IL-22 analysis only) for 4 hours. To block the secretion of cytokines, GolgiStop (BD Biosciences) was added 2 hours after the start of incubation. Dead cells were excluded using Fixable Viability Dye eFluor (eBioscience). Live Cell populations were pre-incubated with an FcγR-blocking monoclonal antibody (anti-mouse CD16/32, 2.4G2, 553142, lot 7248907; BD Biosciences, San Diego, CA) before staining for cell surface antigens. After FcγR blocking, they were stained with antibodies against the indicated cell surface markers, followed by permeabilization in Fix/Perm buffer, and intracellular staining in Perm/Wash buffer (BD Pharmingen) as per kit instructions.

In vivo EdU uptake study

EdU labeling was performed using a Click-iT® Plus EdU Cytometry Assay Kit (Molecular Probes) as previously described (Amiya et al., 2016). Briefly, 400 μg/head EdU was intraperitoneally injected into WT mice for 3 consecutive days. At 1 hour after the last EdU injection, mice were sacrificed and the cells obtained from each organs were analyzed by flow cytometry.

RNA isolation and quantitative real-time PCR

Isolation of total RNA using Trizol reagent (Ambien, USA) was carried out according to the manufacturer's instructions. The complementary DNA was synthesized from the extracted RNA via reverse-transcription using the iScript complementary DNA Synthesis Kit (1708891, lot 64086966; Bio-Rad, Hercules, CA) according to the manufacturer's instructions. The obtained complementary DNA was amplified by quantitative real-time polymerase chain reaction (PCR) using primer sets (Table S1) and the SYBR Green FAST qPCR Master Mix kit (KK4602, lot 004569-4-1; Kapa Biosystems, Wilmington, MA, USA), and gene expression was quantified by comparative cycle threshold method. Rpl32 was used as the internal control, and relative gene expression was determined compared with the expression of internal control. For PCR reactions, samples were first heated to 95°C for 3 minutes, then 40 cycles of the following two steps were applied: 95°C for 3 seconds and 60°C for 20 seconds. The quantitative real-time PCR was performed on the Step OnePlus real-time PCR system (Thermo Fisher Scientific).

Single-cell RNA sequencing (scRNA-seq)

Freshly sorted Treg cells (5,327 Ctrl-Treg and 7,419 IN-Treg) were encapsulated into droplets, and libraries were prepared using Chromium Single Cell 3′ Reagent Kits v2 according to the manufacturer's protocol (10X Genomics). The generated scRNA-Seq libraries were sequenced using a first read of 28 bp and second read of 100 bp (paired-end reads) with a DNBSEQ-G400 (BGI). Sequence reads from all samples were processed by Cell Ranger (10X Genomics). The processed data were aggregated and analysed by Seurat version 3.2.3 (Macosko et al., 2015). Seurat was used to aggregate and analyze the processed data by following the official vignettes (https://satijalab.org/seurat/articles/integration_introduction.html). Specifically, PCA analysis was performed to identify clusters, and 5 gene clusters (0–4) were projected onto UMAP space with the normalized gene expression. A gene expression heatmap was created showing the unbiased generation of the top 10 differentially expressed genes for each cluster (Figure 3D). For scTCR-seq, every clonotype defined using Cell Ranger was identified across all library annotations files and clonotype information was integrated by scRepertoire version 1.3.2 (https://ncborcherding.github.io/vignettes/vignette.html).

Bulk mRNA sequencing

Approximately 20,000–50,000 cells freshly sorted from mice or stimulated with various conditions *in vitro* were lysed with TRIzol (Life Technologies), and total RNA was extracted using Direct-zol RNA MicroPrep (Zymo Research). Total RNA was subsequently processed to generate an mRNA-Seq library using a NEBNext Poly(A) mRNA Magnetic Isolation Module (NEB, E7490S), NEBNext Ultra RNA Library Prep Kit for Illumina (NEB, E7530S) and NEBNext Multiplex Oligos for Illumina (Index Primers Set 1) (NEB, E7335S), according to the protocols provided. The libraries were sequenced for 150 cycles (pair-end read) with a HiSeq 3000 (Illumina). Quality trimming and 3′-end adaptors clipping of sequenced reads were performed simultaneously with trim_galore (v 0.6.4_dev). To quantify transcript abundance, we pseudo-aligned RNA-Seq reads to ENSEMBL transcripts (GRCm38.p6) using salmon (v 1.14.0), and the R package TCC-GUI was used to assess differential gene expression analysis. The normalization method used the trimmed mean of M values (TMM). The differentially expressed gene identification method used was edgeR (cut-off FDR <0.1). Volcano plot were generated using TCC-GUI. Heatmaps were generated in R packages using gplots (v 3.1.1) and pals (v 1.6). Principal components analysis (PCA) and gene ontology (GO) enrichment analysis were generated using TMM values with the iDEP.92 tool (http://bioinformatics.sdstate.edu/idep92/). GO Analysis and Gene Set Enrichment Analysis (GSEA) were performed with clusterProfiler version 4.0.5.

Multi-photon intravital imaging and cell tracking

Nuclei of EC were stained with Hoechst prior to imaging. Animals were anesthetized with 15 mL per gram of 2.5% tribromoethanol (Avertin) and kept on a 1% isoflurane oxygen mixture throughout the procedure. A loop of the terminal ileum was exposed through a

small ventral incision, and the intestine was cut open using a high-temperature disposable cautery pen (Bovie Medical, USA) to expose the mucosal side. The tissue was immobilized in thermal play dough (Laird Technologies, USA) using a lamina attached to a plastic ring containing metal pins. Images were acquired on a A1MP upright multiphoton system (Nikon, Japan) for an average of 30 minutes each. Data were analysed using IMARIS software. Target cells were identified using co-localization for appropriate channel intensities. Auto-regressive tracking algorithms were performed using default settings, and cell tracking was performed using the same algorithm for all samples, including manual verification of correct lymphocyte identification. Cell tracks affected by peristalsis (defined as multiple compartment switches in a short time frame) were excluded automatically (mean percentage of cells excluded over all samples was 5.4 ± 2.4%). Distance was normalized for each movie based on the rendered sizes of the Hoechst-stained IEC nuclei. Where possible, data from multiple crypts in the same movie were pooled.

QUANTIFICATION AND STATISTICAL ANALYSIS

Statistical analyses were performed using Graph-Pad Prism software version 8.0 g (GraphPad). The results are expressed as means $^{\pm}$ SD or $^{\pm}$SEM depending on the number of samples. Groups of data were compared with one-way analysis of variance with the Tukey multiple comparison post hoc analysis or the student t test or Mann–Whitney U test, except for the principal coordinate analysis for the gut microbiome. The differences in the principal coordinate analysis were analysed with the permutational multivariate analysis of variance (PERMANOVA). The difference was considered significant when the p value was less than .05. All of the statistical details of experiments are shown in each figure legend.

Cell Reports, Volume *39*

Supplemental information

Aryl hydrocarbon receptor signals in epithelial cells govern the recruitment and location of Helios^{+} Tregs in the gut

Yusuke Yoshimatsu, Tomohisa Sujino, Kentaro Miyamoto, Yosuke Harada, Shun Tanemoto, Keiko Ono, Satoko Umeda, Kosuke Yoshida, Toshiaki Teratani, Takahiro Suzuki, Yohei Mikami, Nobuhiro Nakamoto, Nobuo Sasaki, Kaoru Takabayashi, Naoki Hosoe, Haruhiko Ogata, Kazuaki Sawada, Takeshi Imamura, Akihiko Yoshimura, and Takanori Kanai

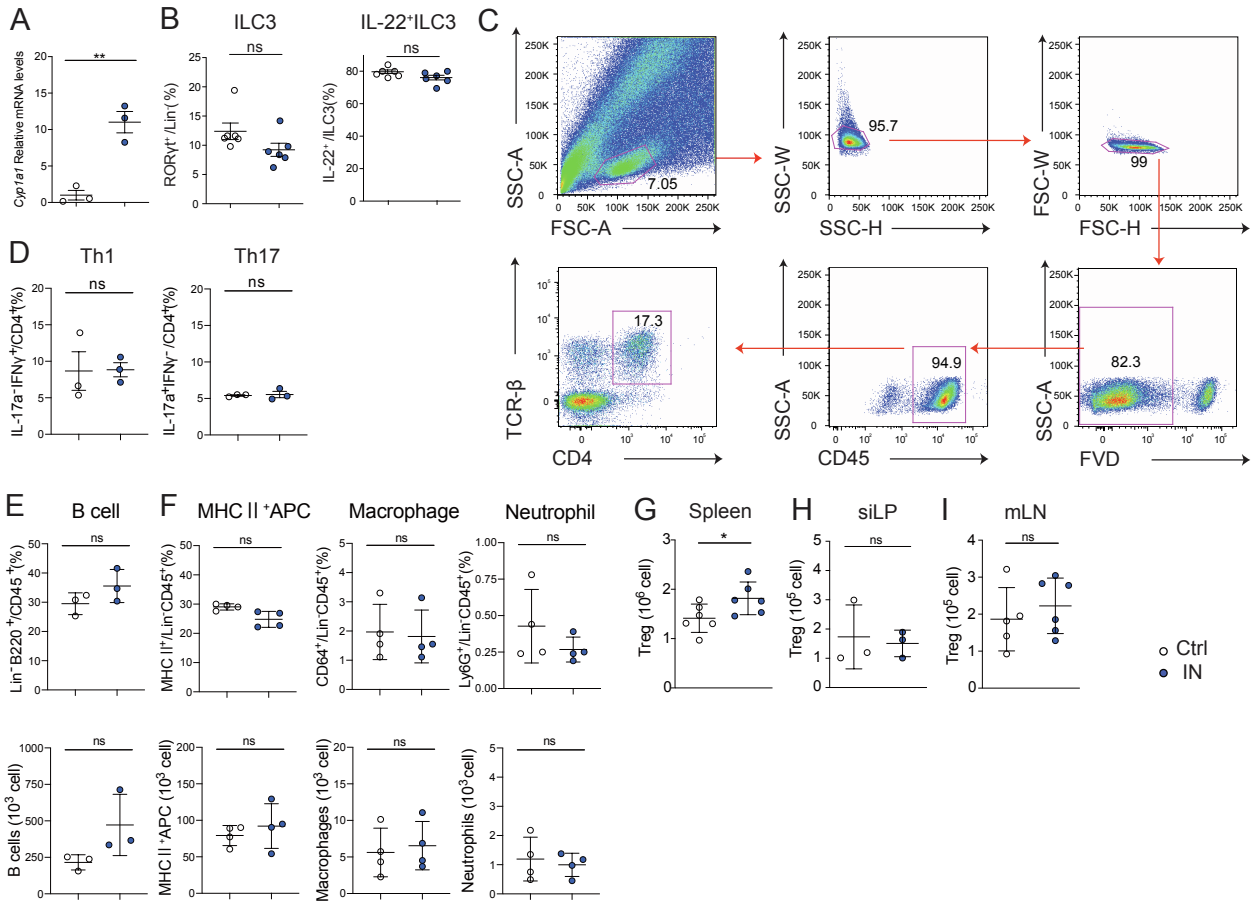

Figure S1. Indigo naturalis does not alter the population of immune cells other than Helios+RORγt- Tregs in colon lamina propria. Related to Figure 1.

C57BL/6J mice of 7-weeks received CE2-diet(Ctrl-diet) or CE2 with 4% indigo naturalis(IN)(IN-diet) for 3 weeks.
A,The mRNA expression of Cyp1a1 gene in colon intestinal epithelial cells were measured. RT-qPCR was performed in triplicate of individual mice (n =3) and *Ct* values obtained were normalized to *Rpl32*. **B,** Percentage of type 3 innate lymphoid cells(ILC3) and IL-22$^+$ cells among CD45$^+$Lin$^-$ cells and ILC3s, respectively, in colon lamina propria(cLP) are shown. Lineage markers are associated with T cells (CD3), B cells (B220), macrophages (CD11b), dendritic cells (CD11c) or neutrophils(Gr-1). **C,**Gating strategy for T cells(FVD$^-$CD45$^+$CD4$^+$TCRβ$^+$). **D,**Percentage of IL-17a$^-$ IFNγ$^+$(Th1)cells and IL-17a$^+$IFNγ$^-$(Th17) cells among CD4$^+$TCRβ$^+$ lymphocyte subsets and number of them are shown.**E,**Percentage of Lin$^-$B220$^+$(B cells) among CD45$^+$cells and number of them are shown.Lineage markers are associated with T cells (CD3) or dead cells (fixable viability dye(FVD)) . **F,**Percentage of MHCII$^+$ (MHCII$^+$ APC), CD64$^+$(macrophages), and Ly6G$^+$(neutrophils) among Lin$^-$CD45$^+$ cells and number of them are shown.Lineage markers are associated with T cells(CD3), B cells (B220 and CD19), NK cells(NK1.1) or dead cells (FVD) .**G-I,** Number of Treg cells in small intestine LP(G), mLN(H), spleen(I) are shown.P values obtained via by student t test. *<0.05,**<0.01, ns: not significant. Data are shown as mean ±SD of individual mice (n = 3-6), representative of two independent experiments.

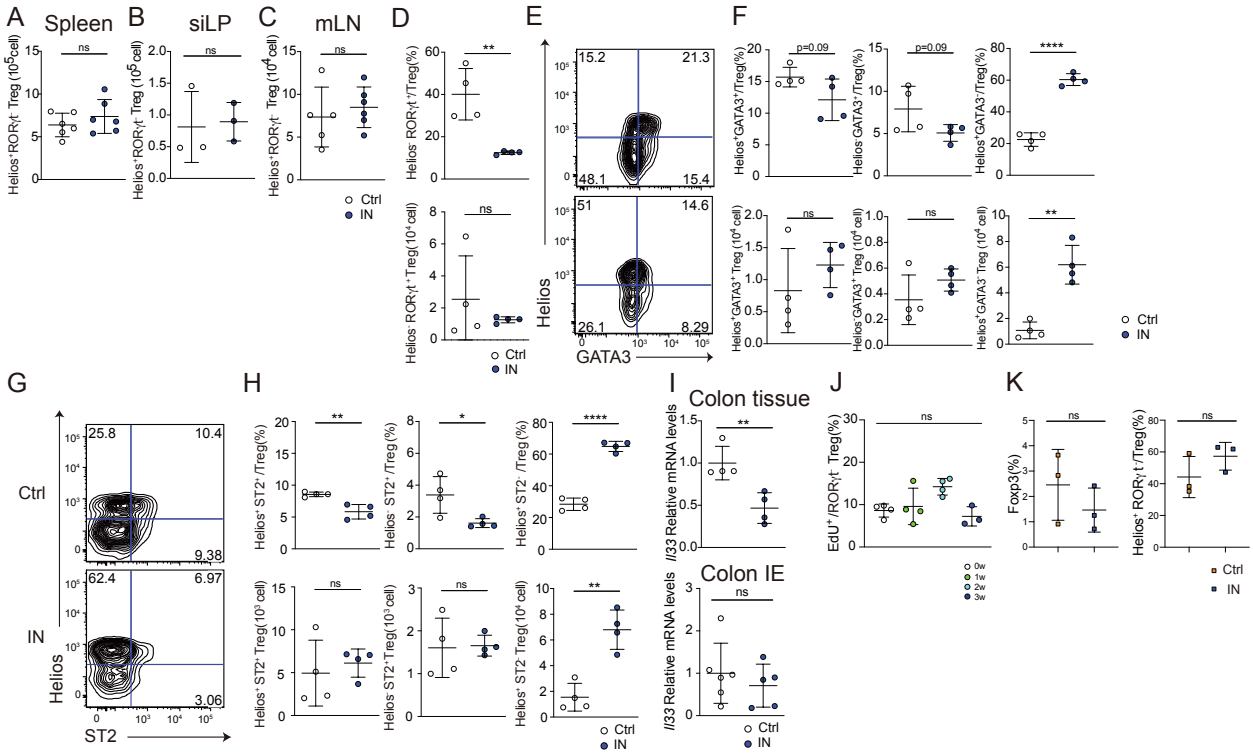

Figure S2. Indigo naturalis specifically induces Helios^{+}RORγt^{-} Tregs in colon lamina propria. Related to Figure 2.

A-I, C57BL/6J mice of 7-weeks received CE2-diet(Ctrl-diet) or CE2 with 4% indigo naturalis(IN)(IN-diet) for 3 weeks. Number of Helios^{+}RORγt^{-} Treg cells in spleen(A) ,small intestine LP(siLP)(B), mLN(C) are shown. Percentage of Helios^{+}RORγt^{-} cells among Treg cell subsets and number of them in colon lamina propria(cLP) are shown(D). Representative flow cytometry plots of Helios and GATA3 expression by Treg cells in cLP(E) , percentage of Helios^{+}GATA3^{+}, Helios^{-}GATA3^{+},and Helios^{+}GATA3^{-} cells among Treg cells and number of them in cLP(F)are shown. Representative flow cytometry plots of Helios and ST2 expression by Treg cells in cLP(G), percentage of Helios^{+}ST2^{+}, Helios^{-}ST2^{+}, and Helios^{+}ST2^{-} cells among Treg cell subsets and number of them in cLP(H) are shown. The mRNA expression of *Il33* gene in colon tissue and colon intestinal epithelial cells were measured(I). **J,** C57BL/6J mice of 7-weeks received Ctrl-diet or IN-diet for a week, 2 weeks, or 3 weeks. EdU(400μg/day) was administered intraperitoneally to them consecutive 3 days from 2 days to 1 hour before the date of sacrifice. Percentage of EdU^{+} cells among RORγt^{+} Treg cells are shown. **K,** CD4^{+}CD45RB^{high} cells (3x10^{5} cells) were transferred into *Rag-2*$^{-/-}$ with Ctrl-diet or IN-diet. Percentage of Foxp3^{+} cells among CD4^{+}TCRβ^{+} lymphocyte subsets and Helios^{+}RORγt^{-} cells among Treg cell subsets of each group in colon are shown. P values obtained via by student t-test(A-D,F,H,I and K) and one-way ANOVA with Tukey's post hoc test(J). *<0.05, **<0.01, ****<0.0001.ns: not significant. Data are shown as mean ± SD of individual mice (n = 3-6), representative of two independent experiments. As for I, RT-qPCR was performed in triplicate of individual mice (n =4) and *Ct* values obtained were normalized to *Rpl32*.

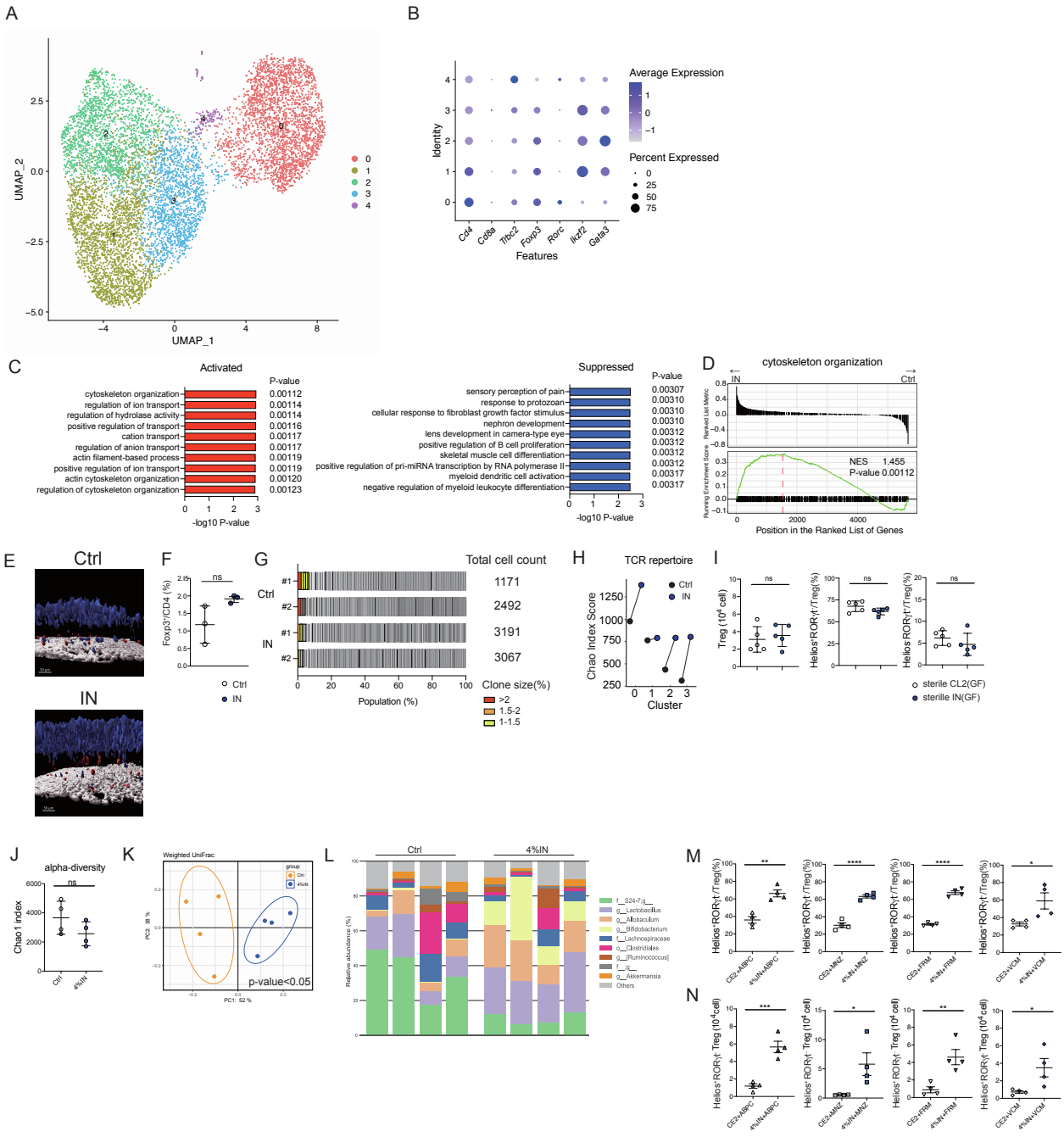

Figure S3. Several phenotypes of Tregs proliferate from multiple cells. Related to Figure 3.

A-D,G, and H, *Rosa26*$^{\text{lsl-tdTomato}}$;*Foxp3*$^{\text{eGFP-Cre-ERT2}}$ mice were treated with TAM administration, and Tomato^{+} CD4^{+} T cells from cLP were sorted for scRNA-Seq using 10X Genomics platform from two mice, which are fed with Ctrl-diet and IN-diet for 3 weeks respectively(n=2/group). UMAP representation of all sequenced cells color coded by cluster. Cluster numbers correspond to colors throughout the figure as indicated(A). Dot plot shows expression of indicated genes in sequenced cells(B). Bar graph shows top enriched biological processes from GO analysis of upregulated or downregulated

genes in IN group compared to Ctrl group(C). Gene set enrichment analysis(GSEA) for gene signatures differntially expressed in IN-Treg versus Ctrl-Treg is shown(D). αβTCR clonal diversity of Tomato^{+} CD4^{+} T cellss in cLP from each sequenced mice are shown. Each slice represents a distinct αβTCR CDR3. Slices are color-coded by clone size(G). Comparison of TCR repertoire diversity between Ctrl- and IN-diet fed mice in each cluster (0-3), which is defined in scRNA-seq data(Fig 3A and FigS3A) was shown(H).**E,** *Rosa26*$^{lsl\text{-}tdTomato}$;*Foxp3*$^{eGFP\text{-}Cre\text{-}ERT2}$ mice were treated with TAM administration, and imaged and reconstructed in 3D imaging with two-photon microscopy (red, Foxp3 ; blue,MHCII; white; SHG). **F,** OT-Ⅱ*Rag2*$^{-/-}$ mice were fed with Ctrl-diet or IN-diet, receiving OVA solution by mixing with drinking water for 3 weeks. Bar graphs for Tregs among CD4^{+} TCRVβ5.1/5.2^{+} cells were shown. **I,** Germ free mice receiving sterile CL2-diet (sterile CL2) or sterile CL2 with sterile 4% IN(sterile IN) for 3 weeks (n=5/group) were analyzed.Percentage of Helios^{+}RORγt^{-} cells among Tregs in cLP, number of Tregs and Helios^{+}RORγt^{-} Tregs are shown. **J-L,** Microbiota composition in faeces of Control- or 4% IN-diet fed mice were analysed using next generation sequencing. Alpha diversity of the gut microbiota(J) the PCoA plots(K) show two groups of subjects (control or 4.0% IN diet) defined by weighted UniFrac microbiota analysis. Taxon-based analysis at the genus level among the groups is shown(L).**M-N,** C57BL/6J mice of 7-weeks received Ctrl-diet or IN-diet for 3 weeks with antibiotics. Each Antibiotics(ampicillin(AMPC), metronidazole(MNZ), neomycin sulfate(FRM), or vancomycin(VCM)) is dissolved in sterile distilled water in the final concentrations described and were administered to mice (500 μL per mouse) by oral gavage 3 times a week. Percentage of Helios^{+}RORγt^{-} cells among Tregs(M) and number of Helios^{+}RORγt^{-} Tregs(N) in cLP are shown. P values obtained via by student t test(F,J,M and N) and permutational multivariate analysis of variance(PERMANOVA)(K). *<0.05, **<0.01, ***<0.001, ****<0.0001. ns: not significant. Data are shown as mean ± SD of individual mice (n = 3-5), representative of two independent experiments. As for E, the image is a representative of three independent sections obtained from two independent experiments.

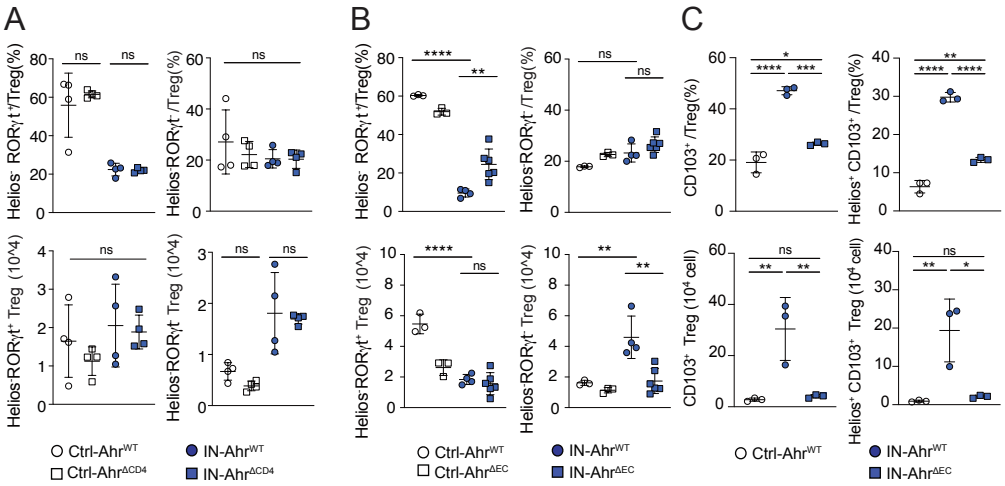

Figure S4. IN accumulate Helios$^+$ Tregs via the AhR signal not in CD4$^+$ cells, but in ECs. Related to Figure 4.

A, TAM(or corn oil as control) pretreated Ahr$^{\Delta CD4}$ mice received Ctrl-diet or IN-diet for 3 weeks(n=4/group), followed by being sacrificed for analysis. Percentage of Helios$^-$ RORγt$^+$ and Helios$^-$RORγt$^-$ cells among Treg cells and number of them in cLP are shown. **B and C,** TAM(or corn oil as control) pretreated Ahr$^{\Delta EC}$ mice received Ctrl-diet or IN-diet for 3 weeks(n=4/group), followed by being sacrificed for analysis. Percentage of Helios$^-$RORγt$^+$, Helios$^-$RORγt$^-$(B), CD103$^+$, and Helios$^+$CD103$^+$ cells(C) among Treg cells and number of them in cLP are shown. P values obtained from one-way ANOVA with Tukey's post hoc test. *<0.05, **<0.01, ***<0.001, ****<0.0001. ns: not significant. Data are shown as mean ± SD of individual mice (n = 3-6), representative of two independent experiments.

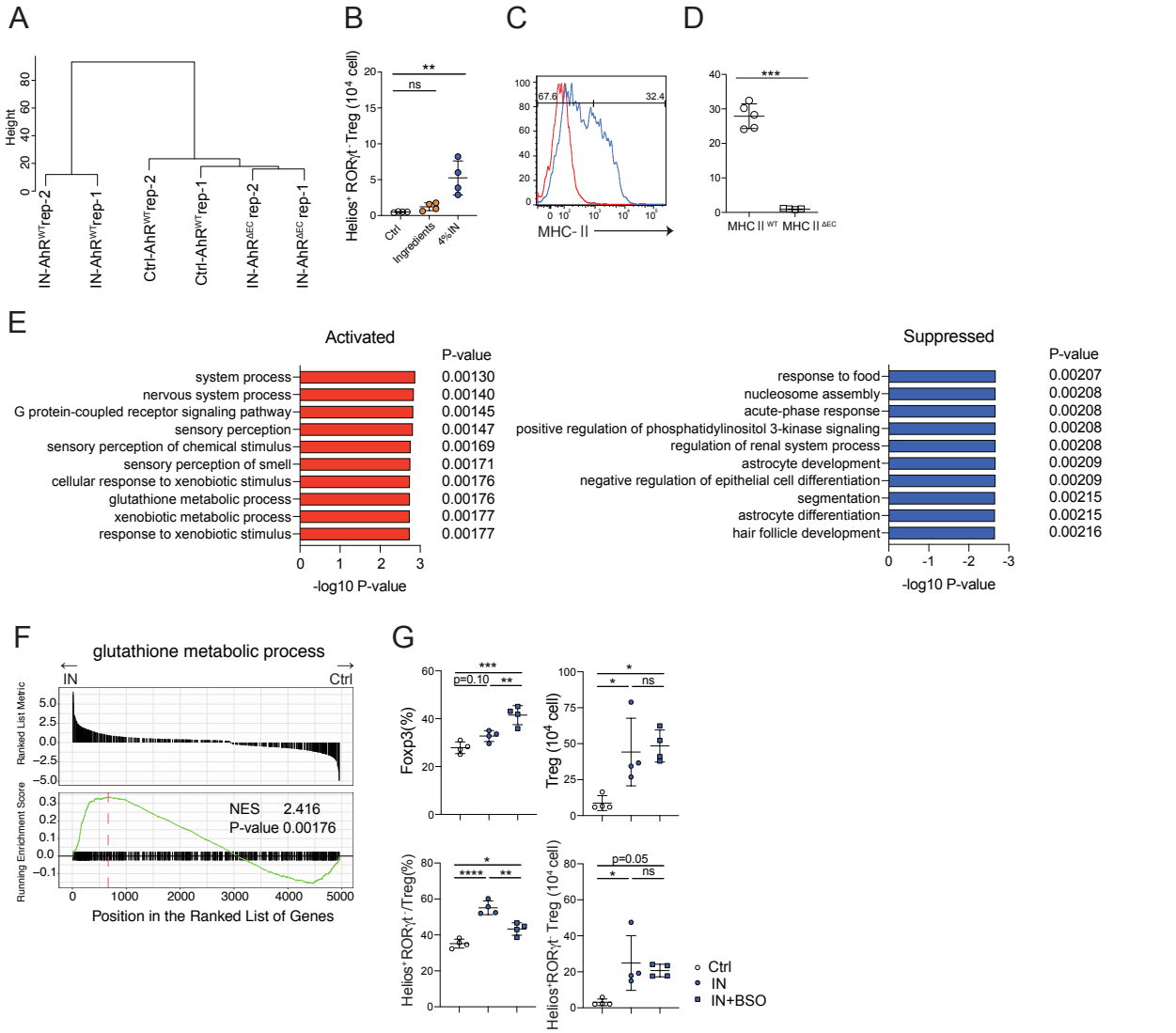

Figure S5. Glutathione did not have an effect on the accumulation of colonic Helios^{+}RORγt^{-} Tregs. Related to Figure 5.

A,E, and F, TAM (or corn oil as control) pretreated Ahr$^{\Delta EC}$ mice received Ctrl-diet(with corn oil(Ctrl-Ahr^{WT})) or IN-diet (with corn oil(IN-Ahr^{WT})or TAM(IN-Ahr$^{\Delta EC}$) for 3 weeks (n=2/group), followed by being sacrificed. Colon ECs(EC) of them were sorted for bulk RNA-Seq. Dendrogram for RNA-seq analyses of ECs in each group is shown(A). Bar graph shows ten enriched biological processes from GO analysis of upregulated or downregulated genes in ECs of IN group compared to those of Ctrl group(E). Gene set enrichment analysis(GSEA) for gene signatures differentially expressed in ECs of IN group compared to those of Ctrl group is shown(F). **B,**C57BL/6J mice of 7-weeks received Ctrl-diet, IN-diet, or CE2 with 4%CaCO3 and oral gavage of DW-suspended substances listed below; indigo(20mg per time),indirubin(0.4mg per time), anthranilic acid(12mg per time), betulin(2mg per time), which are ingredient of IN(Ingredients-group) for 3 weeks (n=4/group) . Number of colon Helios^{+}RORγt^{-} Treg cells of each group are shown. **C and D,** Representative FACS histogram(C) and percentage of MHC class Ⅱ $^{+}$cells(D) among CD45^{-}EpCAM^{+}EC in small intestine of 10-week-old MHC II

^{WT}and MHC II $^{\Delta EC}$ mice are shown. **G,** C57BL/6J mice of 7-weeks received Ctrl-diet, IN-diet, or IN-diet with 5mM buthionine sulphoximine (BSO) in drinking water for 3 weeks (n=4/group). Percentage of Foxp3^{+} cells among CD4^{+}TCRβ^{+}lymphocyte subsets and Helios^{+}RORγt^{-} cells among Treg cell subsets in colon were shown. Number of Treg cells and Helios^{+}RORγt^{-} Tregs in colon were also shown. P values obtained via by one-way ANOVA with Tukey's post hoc test(B and G) and student t test(D). *<0.05, **<0.01, ***<0.001,****<0.0001. ns: not significant. Data are shown as mean $^{\pm}$SD of individual mice (n =4-5), representative of two independent experiments.

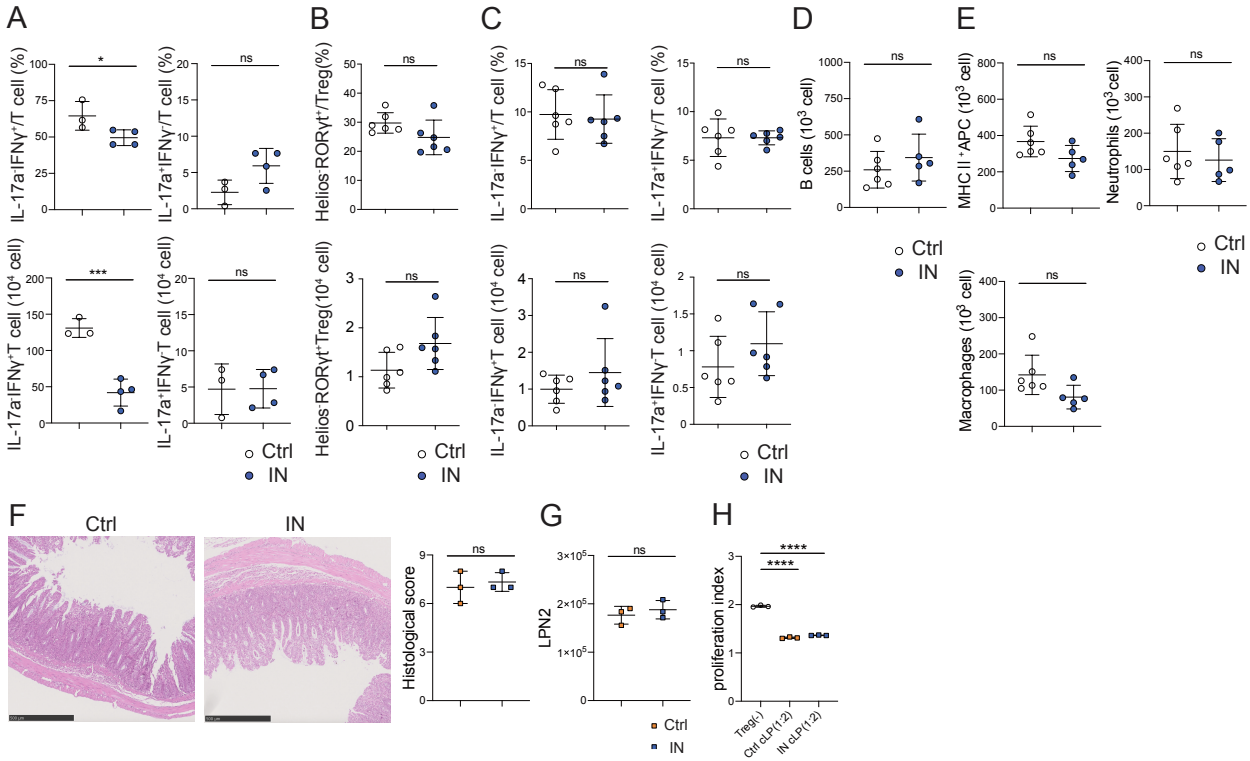

Figure S6. IN does not directly increase the immune cells other than Helios^{+} RORγt^{-} Tregs , and IN-induced Tregs have an suppressive function comparable to Ctrl-Tregs in vitro. Related to Figure 6.

A, *RAG-2*$^{-/-}$ mice were transferred with Ly5.1^{+} CD4^{+}CD45^{RBhigh} cells plus Tomato^{+} CD4^{+} T cells of spleen and mesenteric lymph node obtained from *Rosa26*$^{lsl\text{-}tdTomato}$; *Foxp3* $^{eGFP\text{-}Cre\text{-}ERT2}$ mice, which was treated with TAM administration for consecutive two days, followed by receiving Ctrl-diet or IN-diet for 3 weeks . Mice were sacrificed and analyzed in the 4th week after transfer(n=6-7/group). Percentage of IL-17a^{-} IFNγ^{+}(Th1) cells and IL-17a^{+}IFNγ^{-} (Th17) cells among CD4^{+}TCRβ^{+}subsets in the cLP, and number of them are shown (n=6-7/group). **B-E,** Colon LP cells obtained from C57BL/6J mice, which were fed with Ctrl or 4%IN for 3 weeks (n=6/group) followed by receiving 2% DSS in drinking water are analyzed. Percentage of Helios^{-}RORγt^{+} cells among Treg cell subsets(B,upper) and that of Th1 cells and Th17 cells among CD4^{+}TCRβ^{+}subsets(C, upper) and number of them (B and C,lower) are shown. Number of Lin^{-}B220^{+}(B cells) are shown. Lineage markers are associated with T cells (CD3) or dead cells (fixable viability dye(FVD))(D). Number of MHCII^{+} (MHCII^{+} APC), CD64^{+}(macrophages), and Ly6G^{+}(neutrophils) are shown. Lineage markers are associated with T cells(CD3), B cells (B220 and CD19), NK cells(NK1.1) or dead cells (fixable viability dye(FVD)) (E)(n=5-6/group). **F and G,** CD4+CD45RB^{high} cells (3x10^{5} cells) were transferred into *Rag-2*$^{-/-}$ with Ctrl-diet or IN-diet. Representative H&E stained histological sections from colon(left) and histological scores(right) of each mice(F). Fecal lipicalin-2 levels are shown(G)(These panels are related to Fig.S2K). **H,** Naive CD4^{+} cells were isolated from spleen in C57BL/6J (Ly5.1^{+}) mice using naive CD4^{+}CD62L^{+} T cell isolation kit. Tomato^{+} CD4^{+} T cells of colon lamina propria were obtained from *Rosa26*$^{lsl\text{-}tdTomato}$; *Foxp3*$^{eGFP\text{-}Cre\text{-}ERT2}$ mice. Naive CD4^{+} cells (4×10^{4}) alone or in combination with Tomato^{+} CD4^{+} T cells (2×10^{4}) were cultured in RPMI-1640

medium supplemented with 10% fetal bovine serum, 100 U/ml penicillin, 100 µg/ml streptomycin ,25mM HEPES , 1mM sodium pyruvate, 1x MEM/NEAA and 55µM 2-mercaptoethanol in a 96-well plate. Naive T cells were stimulated in the presence of soluble α-CD3(2 µg/ml) for 3 days with APCs (5×10^4). After incubation, the cells were washed and cell proliferation was assessed by flow cytmetry. P values obtained via by student t-test(A-G) or Dunnett's multiple comparison test(H).**<0.01,****<0.0001, ns: not significant. Data are shown as mean ± SD of individual mice(n=3-6), representative of two independent experiments.

Table S1: Primer sequences for QPCR gene expression assay. Related to Figures S1A, 2E and S2I.

Genes	Forward primer 5'→3'	Reverse primer 5'→3'
Rpl32	ACAATGTCAAGGAGCTGGAG	TTGGGATTGGTGACTCTGATG
Ikzf2	GCCTTTTGAGAGACCTGCTG	TGATGGCTTGGTCCATCATA
Gzma	AGACCGTATATGGCTCTACT	CCCTCACGTGTATATTCATC
Prf1	TTGACTTCAAAAAGGCGCTC	TCTATCTCTGGAGCATCATT
Cyp1a1	GGCCACTTTGACCCTTACAA	CAGGTAACGGAGGACAGGAA
Gzmb	CCACTCTCGACCCTACATGG	GGCCCCCAAAGTGACATTTATT
Il33	ACCAGGTGCTACTACGCTAC	AGTAGTCCTTGTCGTTGGCA